Major, minor and trace element composition of pyromorphite-group minerals as recorder of supergene weathering processes from the Schwarzwald mining district, SW Germany

REVISION 1

Gregor Markl*, Michael A. W. Marks, Johannes Holzäpfel, Thomas Wenzel

Mathematisch-Naturwissenschaftliche Fakultät, Fachbereich Geowissenschaften, Universität Tübingen, Wilhelmstraße 56, D-72074 Tübingen, Germany.

*corresponding author: markl@uni-tuebingen.de

Keywords: pyromorphite, mimetite, vanadinite, fluorophosphohedyphane, hedyphane, trace elements, solid solution, “hydroxylmimetite”

Abstract

More than 150 samples of pyromorphite, mimetite, vanadinite and minerals of the hedyphane-group (which collectively are summarized here under the term PyGM for pyromorphite-group minerals) from the Schwarzwald mining district, SW Germany, have been analyzed by electron microprobe and LA-ICP-MS. In this largest study of its kind, the relations of PyGM composition to host rock and fluid compositions and the amount of solid solution between the various endmembers were investigated. In addition, we report the colors of the many analyzed mineral compositions. The most important results are:

- pyromorphite and mimetite are completely miscible;
- at conditions of the oxidation zone in ore deposits, the solvus between pyromorphite and vanadinite appears to asymmetrical with up to about 3 mol% of vanadinite component in pyromorphite and up to about 39 mol% of pyromorphite component in vanadinite in cases where both minerals coexist;
- due to a lack of suitable samples, the solvus between vanadinite and mimetite could not be completely constrained, but we report vanadinite analyses with up to 12 mol% mimetite and 8 mol% pyromorphite component;
- there is complete miscibility between pyromorphite and phosphohedyphane and between mimetite and hedyphane;
- F-rich varieties appear only to exist in hedyphanes and phosphohedyphanes, while pyromorphites, mimetites and vanadinites are Cl- or OH-dominated;
- we report for the first time analyses suggesting the occurrence of an OH-endmember corresponding to mimetite;
- while pyromorphites are preferably green and mimetites yellow, this is not at all a diagnostic feature, as many exceptions exist; major elements are not correlated at all with the color of a specific crystal;
- most PyGM are strongly zoned and display e. g. significant variations in Ca which are likely to be related to variations of the compositions of various fluid pulses from which the crystals formed;
- PyGM composition is generally uncorrelated with host rock composition, but PyGM enrich other metals like REE, Cr, Sb, Bi or U up to a factor of 10^6; therefore, they can be

regarded as very sensitive recorders of the metal inventory of an oxidation zone and they even record metals only present as traces in the primary ore deposit very reliably;
- REE patterns of PyGM show significant variability even at one location; this may suggest that each zone of a PyGM crystal records the REE pattern of a single fluid pulse or it may indicate fractionation of the REE during PyGM growth; in the absence of conclusive data, the former possibility appears the more likely one;
- PyGM are extremely efficient filters for heavy metals from supergene solutions in and in the vicinity of ore deposits.

Introduction

Pyromorphite-group minerals (PyGM) commonly form during supergene weathering of Pb-bearing ore deposits. The website mindat.org currently lists more than 3000 localities worldwide, with either pyromorphite, mimetite or vanadinite, the respective phosphate, arsenate and vanadate endmembers of the general composition Pb_5X_3Cl occur (X=PO_4^{3-}, AsO_4^{3-} and VO_4^{3-}), plus some dozens of localities for hedyphane-group minerals (hedyphane, phosphohedyphane and fluorphosphohedyphane) which have the composition $Ca_2Pb_3X_3$(Cl, OH, F) with X being either PO_4^{3-}or AsO_4^{3-} (Pasero et al., 2010). Hence, these minerals are ubiquitous and potentially sensitive indicators for processes occurring during oxidation and weathering of ore deposits.

The extent of solid solution between pyromorphite, mimetite and vanadinite has been a long-lasting controversy. Based on the analysis of natural samples, the existence of complete solubility between pyromorphite and mimetite in nature (some of these intermediate, As-rich members even had their own variety name "campylite"; Palache et al., 1951) has long been known (e.g., Denen, 1959; Wondratschek, 1963; Förtsch and Wondratschek, 1965; Cockbain, 1968). The variety "endlichite" (= arsenian vanadinite), describes approximately 1:1 solid solutions of vanadate and arsenate endmembers (Palache et al., 1951).

In the crystal structure of the pyromorphite group minerals two different M sites (two M1 and three M2 sites) with slightly different coordination (9-fold and 7-9-fold, respectively) exist, which plays a role for the hedyphane-group described below (Pasero et al., 2010). The X site is tetrahedrally coordinated. As Pb-O bond lengths do not change much with tetrahedral substitution, Dai and Hughes (1989) inferred that incomplete V-P solid solution at ambient temperature is a consequence of the size difference between V

and P rather than a consequence of the differential distortion of the tetrahedra. Baker (1966) demonstrated the existence of a complete solid solution between pyromorphite, mimetite and vanadinite at 60-80°C based on an X-ray powder diffraction study on twenty-five synthetic compounds grown in this temperature range and recent experimental work showed that complete miscibility along the pyromorphite-vanadinite and the pyromorphite-"*fluorpyromorphite"* joins exists at high temperatures (Chernorukov et al., 2010; Knyazev et al., 2011). To our knowledge, however, no intermediate compositions between phosphate and vanadate endmembers have been reported from natural samples up to now. Baker (1966) suggested that this simply reflects the availability of the respective anions during mineral formation: phosphate and arsenate are relatively common in the oxidized zone of lead deposits and a wide range on phosphate/arsenate ratios are therefore to be expected. According to Baker (1966), however, vanadium is less commonly associated with Pb mineralizations, although the extensive vanadinite and endlichite occurrences in Morocco, Mexico and Arizona argue against this statement. In addition, in the present contribution we report data showing up to 39 % pyromorphite component in natural vanadinite samples.

Members of the hedyphane-group (hedyphane, phosphohedyphane and fluorphosphohedyphane) are characterized by high Ca contents and crystal-chemical studies showed that Ca and Pb are ordered at the two different sites M1 and M2 (e.g., Rouse et al., 1984). Based on the analysis of natural samples, Kempf et al. (2006) showed that Ca and Pb contents show considerable variation but do not exceed the ideal ratio of 2:3. These authors suggested a complete solid solution series among the endmembers pyromorphite-phosphohedyphane and mimetite-hedyphane but the absence of a solid solution series between the joins phosphohedyphane-hedyphane and chlorapatite-turneaureite ($Ca_5(AsO_4)_3Cl$) in natural systems.

In principle, the crystallographic site typically occupied by Cl should also incorporate OH and F. However, a naturally existing F-dominant analogue has been only described (and IMA-approved) for phosphohedyphane (Kempf and Housley, 2011; Pasero et al., 2010). OH-endmembers are not defined to date (Pasero et al., 2010), but Dunn et al. (1985) described OH-bearing hedyphane, while OH-dominated phosphohedyphane is indicated by data from Stalder and Rozendaal (2002). In the present contribution, we report analyses supporting the existence of an OH-endmember of mimetite.

Pyromorphite, mimetite and vanadinite have very low solubility products (log K values of around -75 to -86; Nriagu, 1973; Flis et al., 2007; Bajda 2010; Gerke et al., 2009). For that reason, the use of pyromorphite for treatment and remediation of Pb-contaminated sites by adding phosphate to the soil was suggested (e.g., Ruby et al., 1994; Stanforth and Qui, 2001; Eusden et al., 2002; Basta and McGowen, 2004).

The study of Burmann et al. (2013) used the oxygen isotope composition of phosphate in pyromorphites from some of the localities also used in the present study to decipher the source of the phosphate. The authors came to the conclusion that most of the phosphate has been biologically modified and that no purely inorganic phosphate (e. g. from apatite dissolution in the host rocks of ore deposits) can be identified in pyromorphites.

The present contribution presents a comprehensive dataset of color and geochemical composition from more than 150 samples of PyGM from hydrothermal veins in a large continental mining district, the Schwarzwald (SW Germany). We use major, minor and trace element compositions (including rare earth elements; REE) to detect correlations between host rock composition, primary mineral association of a given hydrothermal vein and fluid source with PyGM geochemistry in order to explore the potential of this ubiquitous mineral group as recorder for fluid-driven processes during weathering of ore deposits.

Samples and geological background

The Schwarzwald in Southern Germany is a low mountain range about 50 by 100 km large (**Fig. 1**). It hosts about 1000 hydrothermal veins, which have been mined since Neolithic and Roman times (Metz et al., 1957; Bliedtner & Martin, 1986); only one mine (the Clara mine near Wolfach) is still exploiting barite and fluorite. The hydrothermal veins contain a large variety of ore assemblages, the most important ones for the present study being galena-sphalerite-chalcopyrite assemblages with minor Bi- or Ni-bearing sulfides in quartz, fluorite, barite or carbonate gangue (**Table 1**). These mineralizations formed more or less continuously over the last 300 Ma (post-Variscan, Pfaff et al., 2009; Staude et al., 2009). The oxidation of the primary ore deposits started about 12 Ma ago, although most supergene minerals are probably younger than 3 Ma (Hofman and Eikenberg, 1991; Hautmann and Lippolt, 2000; Pfaff et al., 2009).

The PyGM-bearing hydrothermal veins are hosted either by basement granites, rhyolites, schists, gneisses and migmatites, or by sandstones of the sedimentary cover (**Table 1**). They occur unevenly distributed in the whole Schwarzwald, with accumulations in the Kinzigtal region (central Schwarzwald) and in the Schauinsland-Münstertal-Todtnau region (southern Schwarzwald). In total, 151 samples from 44 localities have been analyzed (**Fig. 1; Table 1**). They come from quartz-, barite-, fluorite- and carbonate-bearing veins and comprise all different colors from colorless over yellow, orange, green to brown. The textures involve both well-formed prismatic crystals and botryoidal aggregates formed from microcrystalline needles or crusts. Hence, our samples record the variety of mineralization, of textures and of the host rocks present in a typical continental mining district of reasonable geological variety. One additional sample from Beresowsk, Russia, was analyzed to specifically address the question of vanadate-phosphate miscibility in PyGM. This sample shows brown vanadinite overgrowing green pyromorphite crystals up to 5 mm size.

Analytical methods

Electron microprobe (EPMA)

The major and minor element composition of pyromorphite-group minerals was determined using a JEOL 8900 electron microprobe in wavelength-dispersive mode at the Fachbereich Geowissenschaften, Universität Tübingen, Germany. We applied a beam current of 15 nA, an acceleration voltage of 20 kV and a defocused beam of 15 µm diameter. During analyses we permanently controlled the signal and found no increase or decrease during analysis with these conditions applied. The overlap between the Ca Kα and Pb Lγ_1 (4) was corrected for with a factor of 0.008.

Initially, we used PbSe (for Pb), apatite (for Ca, P and F), Zn metal (for Zn), GaAs (for As) and tugtupite ($Na_4AlBeSi_4O_{12}Cl$; for Cl) for calibration. Calculations of the structural formulae (based on 8 cations assuming stoichiometry) showed that using these conditions, As gave reliable results, but Pb was largely under-determined (by up to 30 % relative), whereas P and Cl were strongly over determined. Similar problems were encountered by Eusden et al. (2002) and Fleet et al. (2010). Obviously, a strong matrix effect is present, which cannot fully be corrected for by applying either the ZAF or the $\phi\rho z$ model (Armstrong, 1991). Consequently, matrix-matched calibration standards are

193 needed in order to reliably analyze pyromorphite-group minerals by electron
194 microprobe.
195 Therefore, we externally characterized one pyromorphite (PYR-1 from
196 Schauinsland, Schwarzwald) and a mimetite sample (MIM-1 from Tsumeb, Namibia) in
197 more detail in order to use these materials as calibration standards for microprobe
198 analyses. Detailed SEM and WDS scans showed that in these two samples, only Zn and
199 Ca are present in small amounts (0.06 and 0.35 wt.%, respectively) and that they are
200 homogeneous. For both samples, Pb and As were determined by means of atomic
201 absorption spectroscopy (AAS) and Cl and P were quantified by ion chromatography
202 (IC). These results were used as reference value, are given in **Table 2** and are compared
203 to the theoretical end members. The formula calculations demonstrate the reliability of
204 these data, as the maximum deviations from the theoretical values are generally less
205 than 5 % relative. Based on these tests, we optimized our analytical protocol for the
206 electron microprobe by using PYR-1 and MIM-1 as calibration materials for the major
207 elements (Pb, P, As and Cl). Details of the WDS configuration used, including standards,
208 counting times and the resulting average detection limits are given in **Table 3**.
209
210 LA-ICP-MS
211 Trace elements were analyzed by LA-ICP-MS at the GeoZentrum Nordbayern,
212 Universität Erlangen-Nürnberg, Germany. We used an Agilent 7500i ICP-MS coupled to a
213 UP193FX New Wave Research laser with an output wavelength of 193 nm. Ar was used
214 as carrier gas and ablation was carried out with a pulse rate of 15 Hz and an energy
215 density of 3.5-4.1 and 3.0-3.6 J/cm^2 at spot sizes of 35 and 25 µm, respectively. The
216 software GLITTER 4.0 (Macquarie University) was used for data reduction with NIST
217 SRM610 as the external standard and Pb as the internal standard using microprobe data.
218 Detection limits for most elements were between 0.01 and 0.3 µg/g, depending on the
219 mass number of the element. Higher detection limits were achieved for Si, P, Fe and Zn
220 (105, 8, 7 and 6 µg/g, respectively). The accuracy of concentrations for the reference
221 glass NIST SRM612 was generally within 10 %, except for Tl, which deviates from the
222 literature value (Pearce et al., 1997; GEOREM database) by as much as 34 %,
223 respectively (**Table 4**). As and P concentrations as determined by EPMA and LA-ICP-MS
224 for the same spots give consistent results within error, demonstrating the
225 reproducibility of the two methods.

Results

Major element composition

The results of major element analyses are shown in **Fig. 2,** representative microprobe analyses are given in **Table 5 and 6** and the full data set is available in the **electronic supplement 1**. In accordance with earlier work pyromorphite and mimetite show a complete solid solution series (**Fig. 2 A; Table 5**), while we do not see a complete miscibility with vanadinite. Analyses from sample GM1605 with up to 15 % and from the sample from Beresowsk, Russia, with up to 39% pyromorphite component are the most phosphate-rich natural vanadinite analyses reported so far (**Table 6**). Interestingly, pyromorphite from these vanadinite-bearing samples contains a maximum of 3 % vanadinite component only. **Figure 2** relates the color of an analyzed grain to its major element composition. Although there is a general tendency of green crystals to be phosphate-rich, both orange and yellow colors occur in all compositions irrespective of their P/As ratio.

Most crystals investigated are zoned with respect to their P/As and to their Ca/Pb ratios and this zoning may be continuous and discontinuous **(Fig. 3)**. In cases the substitution of Pb by Ca coincides with a substitution of P by As (**Fig. 3b**) or vice versa (**Fig. 3c and f**), in others not (**Figs. 3a, d and e**). In terms of Ca incorporation, a complete miscibility between both pyromorphite-phosphohedyphane and mimetite-hedyphane (**Fig. 2b**) is observed, but not for the phosphohedyphane-hedyphane join, in accordance with the work of Kempf et al. (2006). The incorporation of Ca is not linked to the type of host rock of the respective hydrothermal vein (**Fig. 4**), although we did not find Ca-rich pyromorphites in sandstones and schists. This, however, may be related to a sample bias (only 2 sandstone and schist samples each were analyzed). The variation in granite and gneiss samples spans the whole range between pyromorphite and phosphohedyphane (and the respective As endmembers).

The vast majority of our analyses are Cl-dominated (**Fig. 5**). Even in fluorite-bearing veins, PyGM are mostly Cl-rich. F-dominance was found in only three samples and these are fluorphosphohedyphanes from fluorite-bearing veins (Gottesehre near Urberg and Haus Baden near Badenweiler). Thus, based on our data, the Cl-F and F-OH exchange seems limited **(Figs. 5 and 6)** even in most fluorite-bearing veins. Our data do allow for drawing a conclusion about the extent of miscibility between F-bearing and F-

free endmembers. In contrast, the Cl-OH exchange appears to be continuous irrespective of the P/As ratio of a PyGM, and we present the (to our knowledge) first microprobe analyses of an near endmember "hydroxylmimetite" in one sample (**Fig. 5 and Table 6**).

Trace element composition

PyGM host a large number of trace elements with large variations and very different median values (**Table 7; electronic supplement 2**). Many trace elements occur in concentrations both significantly lower and higher compared to the bulk continental crust (V, Cr, Cu, Zn, Sr, Y, Mo, Sb, Ba, REE, Y, Bi, Tl and U), others are generally depleted (Mg, Al, Si, Sc, Ti, Mn, Fe, Co, Ni, Th) or enriched (Cd, Ag) when normalized to continental crust values of Rudnick and Gao (2003; **Fig. 7**). Relative enrichment is strongest for Cd, Mo, Ag, Sb, Bi and U (by factors of up to 100 or even 20.000 times) corresponding to absolute concentrations of up to around 2900, 730, 500, 3500, 480 and 5600 µg/g, respectively (**Table 7**). The highest median concentrations were found for Si (250µg/g), U (165µg/g), Zn (91µg/g), Cr (58µg/g) and Y (50µg/g). In contrast, Mg, Co, Ni, Sn, Tl, Bi and Th have very low median concentrations of below 1 µg/g.

Ca exchanges easily with Pb and reaches up to 2 apfu in hedyphane-group members (**Figs. 2-4**). Consistent with literature data (Kempf et al., 2006), significantly higher Ca contents were, however, not observed. In terms of absolute concentrations, Ca strongly dominates over Mg, Sr and Ba, but relative to the total crust, Sr and Ba reach similar enrichment levels as Ca, whereas Mg is always strongly depleted (**Table 7; Figs. 3 and 7**).

Elements potentially exchanging for P, As or V include S, Si, Cr and Mo, assuming that these elements are incorporated in the PyGM structure as tetrahedrally coordinated anions. Relative enrichment of these elements compared to PAAS (Post-archean average australian shale; Taylor and McLennan, 1985) generally increases with ionic radius (Si < Cr < V < Mo; **Fig. 3**; Shannon, 1976). Sulfur is mostly below the electron microprobe detection limit of around 650 µg/g.

The rare earth elements (REE) show strong variations in the shape of PAAS-normalized patterns (**Figs. 3 and 8**; Taylor and McLennan, 1985). The general shape of the patterns varies from LREE-depleted with slightly increasing MREE and HREE to LREE-enriched patterns with flat or decreasing MREE and HREE. The magnitude of the Y anomaly may vary significantly within a single crystal or aggregate (**Fig. 8**). Invariably,

and irrespective of the host rock involved, PyGM have moderately to strongly negative Ce anomalies, while the Eu anomaly is very minor, but mostly positive (**Figs. 8 and 9**).

Figure 10, finally, illustrates the connection between incorporation of the important trace elements Sr, U and again the REE with the occupation of the Pb and the tetrahedrally coordinated site. These results seem to indicate that the incorporation of these trace elements is independent of the crystal chemistry of the PyGM. A weakly positive correlation of Sr and Ca can be noted and will be discussed below, but apart from that, these trace elements occur in all kinds of PyGM irrespective of their major element composition.

Discussion

P-As-V systematics

Our data of PyGM extend, but generally agree with earlier studies on the solid solution behavior of the phosphate, arsenate and vanadate endmembers in nature: while complete miscibility between phosphate and arsenate endmembers is common, miscibility between arsenate or phosphate and vanadate is only observed in few samples and in a quite restricted range. Indeed, some of our samples contain phosphate-bearing vanadinite and almost V-free pyromorphite in close intergrowth (**Fig. 11**). If these phases are in true equilibrium (which is always difficult to ascertain in such low-temperature, fluid-controlled systems), our data imply an asymmetrical solvus. A similar conclusion can be drawn from the observation of almost V-free pyromorphite (up to 3 % vanadinite component only) associated with texturally coexisting descloizite ($PbZn(VO_4)OH$). In one case (sample JH-53), P-bearing vanadinite from the same locality was found in close proximity (but not necessarily textural equilibrium) with pyromorphite and in several samples from the Schauinsland vanadinite overgrown by pyromorphite mimetite solid solutions occurs (**Fig. 11**). These observations indicate that even in the presence of significant vanadium in the supergene solutions, V does not enter pyromorphite, but rather forms distinct vanadate phases. Similar samples exist from Beresowsk, Russia; (**Fig. 11 B)** where vanadinite and pyromorphite overgrow each other with vanadinite containing up to 39 % of pyromorphite component, the pyromorphite, however, only up to 3 % of vanadinite component. Also, some of our samples contain vanadinite and pyromorphite-mimetite solid solutions as distinct

phases. This is in strong contrast to the statement of Baker (1966) who related the absence of V-P solid solution to the absence of V in the vicinity of Pb deposits.

Our data are in agreement with experimental work, which implies complete solid solution along the pyromorphite-vanadinite join at high temperatures above 750°C but indicate that a solvus opens at lower temperatures (Chernorukov et al., 2010), although its exact extent at conditions applicable to supergene processes remains unknown. Our data set shows maximum V contents in pyromorphite, mimetite or a member of the hedyphane group of about 0.8 wt.% V_2O_5 corresponding to about 4 mol% of vanadinite and about 15 % of phosphate or 15 % of arsenate in vanadinite. We assume that our samples formed at or below 30°C (Burmann et al, 2013).

F-Cl-OH systematics

Depending on the conditions of formation (e.g. temperature, pH), the composition of the fluid (e.g. salinity, halogen ratios) and the crystal structure flexibility, the halogen site could in principle be occupied by Cl, F, OH, Br and I. Wondratschek (1963) showed that all possible halogen endmembers of PyGM can be synthesized. However, Br and I endmembers do not play any role in nature, due to the much lower abundance of these elements compared to Cl and F. Interestingly, though, F appears only rarely in PyGM even in samples which come from fluorite-bearing veins and where the analyzed crystals grew on fluorite. This is in accordance with literature data on natural PyGM (e.g., Kempf et al., 2006). Pasero et al. (2010) state that this may be related to the presence of lead (in pyromorphite-mimetite solid solutions) as the dominant cation at both the M1 and M2 sites, which results in larger unit-cell dimensions and makes chlorine (whose ionic radius is markedly greater than those of fluorine and hydroxyl) the best candidate to occupy the X site. The ordering of Ca and Pb at M1 and M2 results in PyGM with Ca of up to 2 apfu with complete miscibility along the pyromorphite-phosphohedyphane and mimetite-hedyphane joins (Kempf et al., 2006). To date it is only in such Ca-rich endmembers that F-dominated compositions were described (Kempf & Housley, 2011; Pasero et al., 2010) and our data confirm this largely (**Figs. 5 and 6**). The mineral fluorophosphohedyphane has only been described in 2011 (Kempf & Housley, 2011), but we also found it in the course of our study. It may thus not be as previously assumed. On the other hand, Cl-OH exchange appears to be continuous and in addition to the already described hydroxylpyromorphite, we suggest that our analyses

357 from sample LK5 are clear indication of the existence of the mineral "hydroxylmimetite"
358 (**Fig. 5**).
359
360 Pb-Ca-Sr systematics
361 The only important cation substituting for Pb on the M1 site is Ca (**Fig. 3**). According to
362 the zoning patterns shown in **Fig. 3**, strong variations of the Pb/Ca ratio may occur
363 within a single crystal. These variations may be continuous (e. g. **Fig. 3a**) or
364 discontinuous (e. g. **Fig. 3e**). While the source of Pb is invariably the ore deposit
365 undergoing oxidation, the source of Ca can be either a Ca-bearing phase in the ore
366 deposit (e.g., calcite or fluorite) or weathering plagioclase or a different mineral in the
367 host rock. We speculate that a sudden increase in Ca may be related to a major influx of
368 new, Ca-bearing water, which undergoes subsequent closed-system fractionation (i. e.,
369 desiccation). This could lead to smooth Pb-Ca zoning in a given crystal. If this is true,
370 PyGM zoning would record major fluid influx events into a system undergoing oxidation.
371 The weak positive correlation of Sr with Ca (**Fig. 10**) indicates either a crystal
372 chemical effect or a common source of these elements, which are transported to the site
373 of PyGM formation in the meteoric fluid. While a crystal chemical effect appears unlikely
374 given the amazing elasticity of the PyGM structure for all sizes of trace element ions, a
375 common source for Ca and Sr appears reasonable. In principle, Ca and Sr could be set
376 free during plagioclase weathering in the host rocks, or during weathering of
377 carbonates, fluorite and barite gangue within the hydrothermal vein itself. It is at
378 present impossible to distinguish between these two possibilities.
379
380 Trace metals
381 The high concentrations of Cu (up to 2240µg/g), Zn (up to 8600µg/g), Cd (up to
382 2920µg/g), Sb (up to 3770µg/g) and Ag (up to 510µg/g) in PyGM (**Table 7**) are not
383 really surprising as these elements are present in the main ore minerals (such as
384 chalcopyrite (Cu), sphalerite (Zn, Cd) and galena (Ag, Sb)) in the investigated deposits.
385 The high concentrations of Bi (up to 480 µg/g) are at first glance surprising, as
386 this element is not so typically related to these kinds of ores. However, the highest Bi
387 concentrations in our sample set come from the Herrensegen and Urberg mines
388 (samples JH-95 and JH-13), which are both known for their occurrence of Bi-bearing
389 sulfides (e.g., Walenta, 1992; Staude et al., 2010). Indeed, bismuth is a perfect element to

illustrate the capability of PyGM to record the average element inventory of a given ore deposit, because the fluids they form from potentially integrate over a significant portion of the ore deposit before precipitating PyGM. For example, at the Urberg locality only trace amounts of Bi-bearing sulfides are present (based on the findings of hundreds of mineral collectors over tens of years and based on the careful examination of dozens of polished ore sections). Nevertheless, PyGM invariably show significant Bi concentrations. This indicates that PyGM are able to record the entire element inventory of a given ore deposit which otherwise would be difficult to assess from microscopic examination of the ore minerals.

In contrast to the aforementioned trace elements, U (up to 5600µg/g) shows no correlation with the element inventory of the specific hydrothermal vein the PyGM are related to. Hence, elevated concentrations of U most probably reflect mobilized U from the country rocks transported by the meteoric fluid to the site of PyGM precipitation. U-rich PyGM from the Schwarzwald was already described by Kirchheimer (1957). Mine water analyses of Göb et al. (2013) report maximum U contents of about 0.07 mg/l, while the U concentrations in PyGM reach 5600 µg/g. Thus, the uranium partition coefficient D_U between PyGM is between 100 and about $5*10^6$ and PyGM may act as natural barriers for U-bearing water (**Fig. 12)**. The same holds true for other potentially toxic elements like Cr ($D_{Cr} = 1*10^4$-$7*10^6$), Tl ($D_{Tl} = 70$-$3*10^5$), Bi ($D_{Bi} = 2*10^4$-$2*10^6$), Ag ($D_{Ag} = 50$-$2*10^6$), Cu ($D_{Cu} = 100$-$2*10^4$), Cd ($D_{Cd}=30$-$1*10^4$), Sb ($D_{Sb} = 30$-2000).

Rare Earth Elements

The REE patterns of PyGM show a number of features, which need to be discussed. These concern the Ce- Eu- and Y anomalies and the general shape of the REE patterns compared to those of mine water from the corresponding localities. The latter ones are taken from the extensive studies of Göb et al. (2011 and 2013). We explicitly state that although the water samples of their study were taken from the same localities from which the PyGM samples of the present study are derived, it was not possible to sample the exact fluid the PyGM grew from (as they probably grew thousands or even millions of years ago). It is, however, not unreasonable to assume that the oxidation zone fluids at the time of growth and those today are similar. Hence, we will compare the REE composition of PyGM to water REE compositions for localities where we have both mineral and water analyses available. These are the Clara and Friedrich-Christian mines

in the central Schwarzwald, and the Kammendobel and Schauinsland localities in the Southern Schwarzwald **(Fig. 13)**. At the latter two localities, pyromorphite sinters grow today in the mines from which we sampled fluids dripping out of fractures in the hydrothermal veins (however, unfortunately, not exactly from the place where the sinters grew). These fluids are regarded as oxidation zone fluids rather than (mixed, stagnant or free-flowing) mine waters. In principle, two different types of PyGM patterns exist: some are very similar to the respective water pattern (e. g. **Fig. 13C** and some in **Fig. 13D**), while others show slight to significant differences. We interpret the similarity of e. g. sample JH-88 in **Fig. 13D** with the host rock water from the Clara vein to reflect precipitation of the PyGM crystals from a water with an element enrichment pattern similar to that found in PyGM (as it is very unlikely that it is pure coincidence). This is even more reasonable, as the host rock composition has certainly not changed over the last thousands of years and hence, the REE composition of the host rock water is very likely to have been rather similar over this time span. In contrast, water flowing through the hydrothermal vein may show stronger variations as hydrothermal veins are rather heterogeneous and may contain different assemblages of ores and gangue minerals at various locations within the vein. We state that none of the PyGM analyses shows systematic deviations from the respective mine waters (with the exception of Ce and Y which will be dealt with below), i. e., we see various deviations, but there is no systematics behind them as we would it expect it, if fractionation of the various REE from each other played a role. The only systematic difference is the difference in concentration between PyGM and water samples. The close similarity of some of the PyGM with some of the water patterns and the variations both in water and in PyGM REE geochemistry at one locality (see also Göb et al., 2011 and 2013) implies that each analysis of a PyGM reflects the REE composition of one specific fluid pulse (except for Ce and Y, see below). If this were true, the PyGM would be perfect recorders of REE variability in natural waters which is particularly interesting as REE concentrations in PyGM are by a factor of about 10^6-10^7 higher than in the natural waters (**Fig. 13**) and analysis is therefore much simpler.

Ce anomalies in PyGM are typically more strongly negative than those of the meteoric waters from which the PyGM precipitated (**Fig. 13**). Most likely, this is caused by preferential partitioning of Ce(IV) into Fe-Mn oxides (e. g., Loges et al., 2012) that commonly form in the vicinity of PyGM or along the flow paths of the water. The PyGM

show slightly positive, negative or no Y anomalies, while all water analyses show slightly positive anomalies (**Fig. 13**). Hence, PyGM are not suited to monitor the chemical behaviour of Y in the water. The Eu anomaly of the meteoric fluid, in contrast, seems to be well recorded by the PyGM (compare with the data of Göb et al., 2013), which may be of help to deduce fluid pathways in complex geological situations with strongly contrasting lithologies involved (e. g., sandstone cover on granitic basement rocks; **Fig. 9**).

Implications

The strong zoning apparent in most analyzed crystals or aggregates is interpreted to reflect single episodes of fluid flow and weathering during the textural evolution of an oxidized ore deposit. If this is so and a homogeneous, some tens of micrometers thick zone reflects e. g. a period of intensified water influx into an oxidized vein or, quite opposite, a dry period, then PyGM could be able to record very sensitively these surface processes. Furthermore, due to their extremely low solubility products, they keep this information for a long time and probably even during fluvial transport. The growth of pyromorphite is invariably related to microbial transformation of phosphate ions (Burmann et al., 2013). These minerals form a bridge between a physical surface process such as rain or snow melt, the microbial interaction with this circulating surface water, and the transport and precipitation of heavy metals typically (but not necessarily) derived from weathered inorganic ore deposits. Unfortunately, attempts to use PyGM for age dating using fission track or U/Th-He methods have not succeeded yet.

Another interesting application of PyGM may lie in the reconstruction of trace element compositions of paleofluids at localities, where supergene processes can be dated using different minerals (e. g. Mn oxides), which are coeval with the PyGM. As **Fig. 13** shows, the relative enrichment patterns of the REE found in PyGM (with the exception of Ce and Y, the latter being not a REE anyway) are similar to almost identical to those of meteoric waters from the same mine. As REE analyses in meteoric water are extremely difficult (due to the very low concentrations in the ng/l range, Göb et al., 2013), LA-ICP-MS analyses of PyGM would be a much easier way to reconstruct them, at least qualitatively. The same may hold true for other trace elements **(Fig. 12)** and thus may render PyGM an interesting prospecting tool, especially regarding the potential to reconstruct the bulk element inventory of a specific ore deposit based on the relative

abundances of e. g. heavy metals in PyGM. Experimental determination of partition coefficients for important fluid-mobile elements including U, the heavy metals and the halogens would be next steps to establish PyGM as important tools in low-temperature geochemistry. This is especially desirable, as these minerals act as powerful barriers for a large variety of toxic metals (e. g. Cr, Tl, Cd) in addition to their ability to immobilize Pb and As (Ruby et al., 1994; Stanforth and Qui, 2001; Eusden et al., 2002; Basta and McGowen, 2004).

Acknowledgements

The vanadinite sample from Beresowsk was provided by Dr. Renate Schumacher from the Mineralogisches Museum im Poppelsdorfer Schloß, Bonn. This is gratefully acknowledged. We are also grateful to Indra Gill-Kopp and Per Jeisecke for the careful preparation of polished thin sections and to Max Keim, Linda Krahé and Helene Brätz for their friendly help with mineral analyses. Two anonymous reviewers provided thoughtful reviews which are very gratefully acknowledged, as they not only improved the present paper, but also initiated the idea for another study on this fascinating mineral group.

References

Armstrong J. T. (1991) Quantitative elemental analysis of individual microparticles with electron beam instruments. In: Heinrich, KFJ & Newbury, DE (eds), Electron Probe Quantitation New York & London: Plenum Press, 261-315

Badja T. (2010) Solubility of mimetite Pb5(AsO4)3Cl at 5-55°C. Environmental Chemistry, 7, 268-278

Baker W. E. (1966) An X-ray diffraction study of synthetic mwmbers of the Pyromorphite Series. The American Mineralogist 51:1712-1721

Basta N. and McGowen S. (2004) Evaluation of chemical immobilization treatments for reducing heavy metal transport in a smelter-contaminated soil. Environmental pullution, 127, 73-82

Bliedtner M. and Martin M. (1986) Erz- und Minerallagerstätten des mittleren Schwarzwaldes. LGBR, Freiburg, 686 p.

Burmann F., Keim M. F., Oelmann Y., Teiber H., Marks M., and Markl G. (2013) The source of phosphate in the oxidation zone of ore deposits: evidence from oxygen isotope compositions of pyromorphite. Geochimica Cosmochimica Acta. 123, 427-439.

Chernorukov N. G. , Knyazev A. V., and Bulanov E. N. (2010) Isomorphism and Phase Diagram of the $Pb_5(PO_4)_3Cl$-$Pb_5(VO_4)_3Cl$ System. Russian Journal of Inorganic chemistry, 55, 1463-1470

Cockbain A. G. (1968) The crystal chemistry of the apatites. Mineralogical Magazine, 37, 654-660

Dai, Y. and Hughes, J. M. (1989) Crystal-structure refinements of vanadinite and pyromorphite. Canadian Mineralogist, 27, 189-192

Denen W. H. (1959) Principles of Mineralogy. The Ronald Press Co, New York

Dunn P. J., Rouse R. C., and Nelen J. A. (1985) Hydroxyl-bearing hedyphane from Långban, Sweden. Geol Fören Stockholm Förhandlinger, 107, 325-327

Eusden J. D., Gallagher L., Eighmy T. T., Crannell B. S., Krzanowski J. R., Butler L. G., Cartledge F. K., Emery E. F., and Francis C. A. (2002) Petrographic and spectroscopic characterization of phosphate-stabilized mine tailings from Leadville, Colorado. Waste Management, 22, 117-135

Fleet M. E., X. L., and Shieh S. R. (2010) Structural change in lead fluorapatite at high pressure. Physics and Chemistry of Minerals, 37, 1-9

Flis J., Manecki M., and Badja T. (2007) Solubility of pyromorphite-mimetite solid solutions at 5-65°C. Geochimica Cosmochimica Acta Supplement, 71, 285

Förtsch E. and Wondratschek H. (1965) Zur Kristallchemie der Minerale der Pyromorphit-Gruppe. Die Naturwissenschaften, 52, 182

Gerke T. L., Scheckel K. G., and Schock M. R. (2009) Identification and Distribution of Vanadinite ($Pb_5(VO_4)_3Cl$) in Lead Pipe Corrosion By-Products. Envinonmental Science and Technology, 43, 4412-4418

Göb S., Wenzel T., Bau M., Jacob D. E., Loges A., and Markl G. (2011) The redistribution of rare-earth elements in secondary minerals of hydrothermal veins, Schwarzwald, Southwestern Germany. The Canadian Mineralogist, 49, 1305-1333.

Göb S., Loges A., Nolde N., Bau M., Jacob D. E., and Markl G. (2013) Major and trace element compositions (including REE) of mineral, thermal, mine and surface waters in SW Germany and implications for water-rock interaction. Applied Geochemistry, 33, 127-152

Hautmann S. and Lippolt H. J. (2000) $^{40}Ar/^{39}Ar$ dating of central European K-Mn oxides – a chronological framework of supergene alteration processes during the Neogen. Chemical Geology, 170, 37-80

Hofmann B. and Eikenberg J. (1991) The Krunkelbach uranium deposit, Schwarzwald, Germany: correlation of radiometric ages (U-Pb, U-Xe-Kr, K-Ar, ^{230}Th-^{234}U) with mineralogical stages and fluid inclusions. Economic Geology, 86, 1031-1049

Kalt A., Altherr R., and Hanel M. (2000) The Variscan basement of the Schwarzwald. European Journal of Mineralogy Beihefte, 12, 1-43

Kempf A. R. and Housley R. M. (2011) Fluorphosphohedyphane, $Ca_2Pb_3(PO_4)_3F$, the first apatite supergroup mineral with essential Pb and F. The American Mineralogist, 96, 423-429

Kempf A. R., Steele I. M., and Jenkins R. A. (2006) Phosphohedyphane, $Ca_2Pb_3(PO_4)_3Cl$, the phosphate analog of hedyphane: description and crystal structure. The American Mineralogist, 91, 1909-1917

Kirchheimer, F. (1957) Bericht über das Vorkommen von Uran in Baden-Württemberg. Abh. Geol. Landesamt Baden-Württemberg, 2, 1-127.

Knyazev A. V., Chernorukov N. G., and Bulanov E. N. (2011) Isomorphism and phase diagram of $Pb_5(PO_4)F$-$Pb_5(PO_4)_3Cl$ system. Thermochimica Acta, 513, 112-118

Loges A., Wagner T., Barth M., Bau M., Göb S., and Markl G. (2012) Negative Ce anomalies in Mn oxides: the role of Ce^{4+} mobility during water–mineral interaction. Geochimica Cosmochimica Acta, 86, 296-317

Metz R., Richter M., and Schürenberg H. (1957) Die Blei-Zink-Erzgänge des Schwarzwaldes. Beihefte zum Geologischen Jahrbuch, 1, 1-277

Nriagu J. O. (1973) Lead orthophosphates-II. Stability of chlorpyromorphite at 25°C. Geochimica Cosmochimica Acta, 37, 367-377

Palache C., Berman H., and Fondel C. (1951) The System of Mineralogy of James Dwight Dana and Edward Salisbury Dana, Yale University 1837-1892, Volume II. John Wiley and Sons, Inc, New York, 7th edition, revised and enlarged, 1124 pp

Pasero M., Kampf A. R., Ferraris C., Pekov I. V., Rokovan J., and White T. J. (2010) Nomenclature of the apatite supergroup minerals. European Journal of Mineralogy, 22, 163-179

Pearce N., Perkins W., Westgate J. A., Gorton M. P., Jackson S. E., Neal C. R., and Chenery S. P. (1997) A compilation of new and published major and trace element data for NIST SRM

610 and NIST SRM 612 glass reference materials. Geostandards Newsletter, 21, 115-144

Pfaff K., Romer R. L., and Markl G. (2009) U-Pb ages of ferberite, chalcedony, agate, `U-mica' and pitchblende: constraints on the mineralization history of the Schwarzwald ore district. . European Journal of Mineralogy, 21, 817-836

Rouse R. C., Dunn P. J., and Peacor D. R. (1984) Hedyphane from Franklin, New Jersey and Långban, Sweden: cation ordering in an arsenate apatite. The American Mineralogist, 69, 920-927

Ruby M. V., Davis A., and Nicholson A. (1994) In Situ Formation of Lead Phosphates in Soils as a Method to Immobilize Lead. . Envinonmental Science and Technology, 28, 646-654

Rudnick R. L. and Gao S. (2003) Composition of the continental crust. In: Rudnick, R. L. (ed), The crust, Vol 3 of Treatise on geochemistry (eds HD Holland & KK Turekian), Elsevier-Pergamon, Oxford, vol., pp 1-64.

Shannon R. D. (1976) Revised effective ionic radii and systematic studies of interatomic distances in halides and chalcogenides. Acta Crystallographica, 32, 751-767

Stalder M. and Rozendaal A. (2002) Graftonite in phosphatic iron formations associated with the mid-Proterozoic Zn-Pb deposit, Namaqua province, South Africa. Mineralogical Magazine, 66, 915-927

Stanforth R. and Qui J. (2001) Effect of phosphate treatment on the solubility of lead in contaminated soil. Environmental Geology, 41, 1-10

Staude S., Bons P., and Markl G. (2009) Hydrothermal vein formation by extension-driven dewatering of the middle crust: An example from SW Germany. Earth and Planetary Science Letters, 286, 387-395

Staude S., Dorn A., Pfaff K., and Markl G. (2010) Assemblages of Ag-Bi sulfosalts and conditions of their formation: the type locality of schapbachite ($Ag_{0.4}Pb_{0.2}Bi_{0.4}S$) and neighboring mines in the Schwarzwald ore district, Southern Germany. The Canadian Mineralogist, 48, 441-466

Taylor S. R. and McLennan S. M. (1985) The continental crust: its composition and evolution. Blackwell Scientific Publications, Oxford

Walenta K. (1992) Die Mineralien des Schwarzwaldes und ihre Fundstellen. Weise Verlag, München

Wondratschek H. (1963) Untersuchngen zur Kristallchemie der Blei-Apatite (Pyromorphite). Neues Jahrbuch für Mineralogie Abhandlungen, 99, 113-160

Figure Captions

Figure 1: Simplified geological map of the Schwarzwald (modified after Kalt et al., 2000) with sample localities as given in Table 1. Abbreviations: BLZ and BBZ: Badenweiler-Lenzkirch and Baden-Baden-Gaggenau-Zones; SSGC and CSGC: Southern and Central Schwarzwald Gneiss Complexes.

Figure 2: Classification of Pyromorphite-group minerals. (A) Analyses of the present study in the ternary system pyromorphite-mimetite-vanadinite. The color-coding approximates the colors of the crystals in which a specific analysis was done. (B) The

628 same analyses plotted in the trapezoid pyromorphite-mimetite-hedyphane-
629 phosphohedyphane.
630
631 **Figure 3:** Examples of zoning textures (BSE images) of PyGM found in the present
632 sample set combined with major and trace element data. In some cases the substitution
633 of Pb by Ca coincides with a substitution of P by As (**B**) or vice versa (**C and F**), in others
634 not (**A, D and E**).
635
636 **Figure 4:** Ca content of PyGM from the Schwarzwald related to the host rock of the
637 respective hydrothermal vein.
638
639 **Figure 5: (A) – (C):** F-Cl-OH systematics of PyGM of the present study. Almost all
640 samples contain Cl-dominated PyGM (A). In three samples (JH-17, JH-18 and JH-129)
641 fluorphosphohedyphane was found (B) and one sample (LK5, C) contains halogen
642 deficient mimetite indicating the presence of a potential *"hydroxylmimetite"* end
643 member. (D): BSE image of sample LK5 from the Michael mine. Grey crystals are PyGM,
644 the three white lines show analytical traverses along which the analyses shown in (C)
645 were done. Black areas are quartz.
646
647 **Figure 6:** Ca-F-Cl systematics of PyGM as analyzed in the present study. (A) Most
648 samples are F-free or F-poor, only at high Ca ccontents, F-rich compositions were found
649 (fluorphosphohedyphane). (B) Plot illustrating the exchange of Cl with F.
650
651 **Figure 7:** Crust-normalized trace element patterns for the whole sample set.
652 Normalizing values after Rudnick &and Gao (2003). Most trace elements occur in highly
653 variable concentrations both lower and higher compared to the bulk crust (V, Cr, Cu, Zn,
654 Sr, Y, Mo, Sb, Ba, REE, Y, Bi, Tl and U), others are generally depleted (Mg, Al, Si, Sc, Ti, Mn,
655 Fe, Co, Ni, Th) or enriched (Cd, Ag).
656
657 **Figure 8:** Examples of PAAS-normalized rare earth element (REE) patterns for PyGM
658 from the Schwarzwald, showing strong variation in the general shape of the patterns.
659

Figure 9: Ce- and Eu-anomalies for PyGM from the Schwarzwald related to the host rock of the respective hydrothermal vein.

Figure 10: Correlations of (A) Sr, (B) U and (C) REE contents with the occupation of the Pb-Ca and the P-As site, expressed as Ca# and P#, respectively.

Figure 11: PyGM analyses of the present study in the ternary system pyromorphite-mimetite-vanadinite from the Feldberg (A) and from Beresowsk in Russia (B) and reflected light images (WOP = 430 µm) of vanadinite (white) overgrown by pyromorphite (pale gray) from the Schauinsland (C) and (D).

Figure 12: Trace elements in PyGM normalized against water from the respective locality (water data from Göb et al., 2011 and 2013).

Figure 13: PAAS-normalized REE patterns of selected PyGMs (no recent sinters, but oxidation zone samples) compared to the REE pattern of waters from the same mines (water data from Göb et al., 2011 and 2013).

Figure 1

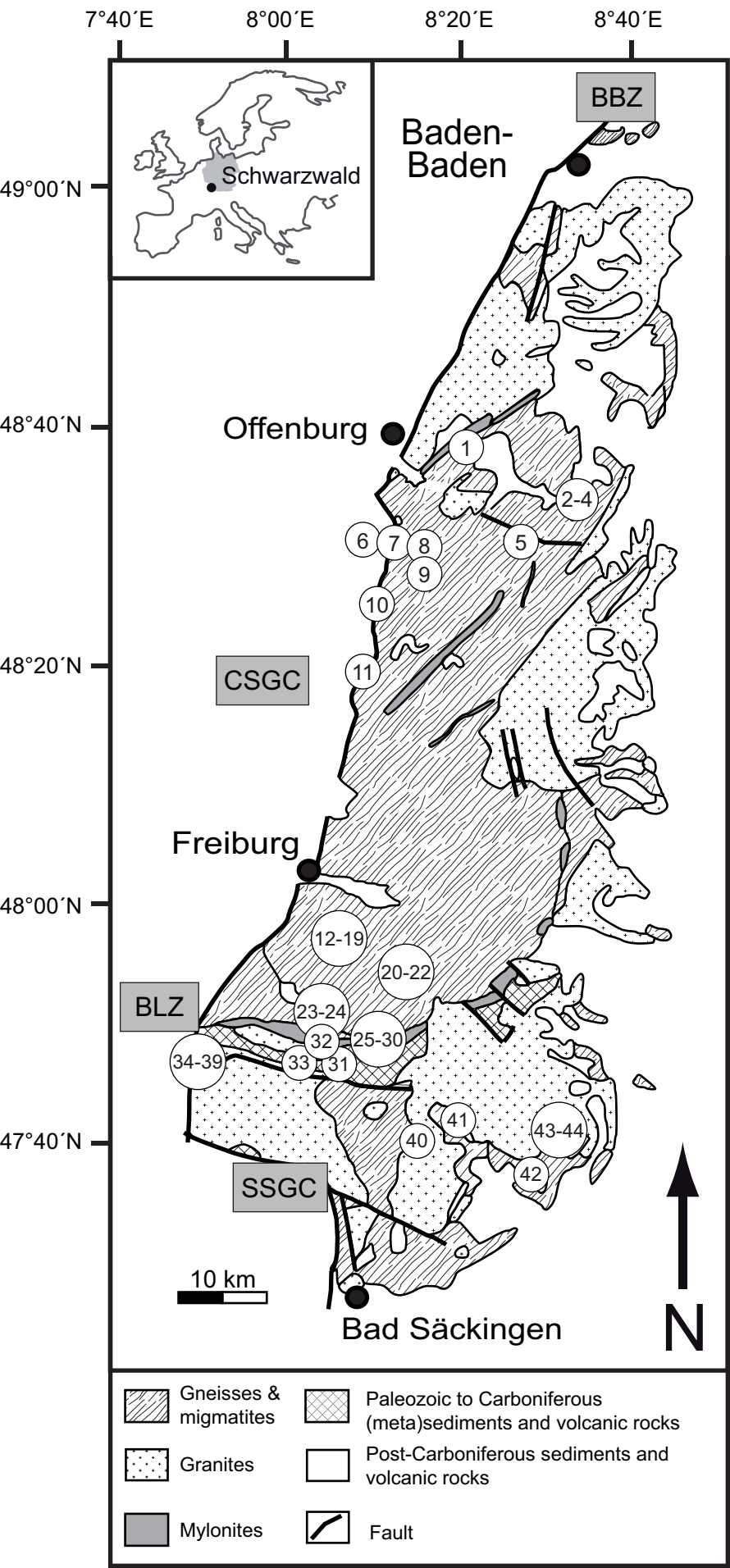
7°40´E
8°00´E
8°20´E
8°40´E
49°00´N
48°40´N
48°20´N
48°00´N
47°40´N
Schwarzwald
BBZ
Baden-
Baden
Offenburg
CSGC
Freiburg
BLZ
SSGC
Bad Säckingen
1
2-4
5
6
7
8
9
10
11
12-19
20-22
23-24
25-30
31
32
33
34-39
40
41
42
43-44
10 km
N
Gneisses & migmatites
Granites
Mylonites
Paleozoic to Carboniferous (meta)sediments and volcanic rocks
Post-Carboniferous sediments and volcanic rocks
Fault

Figure 2

(A)

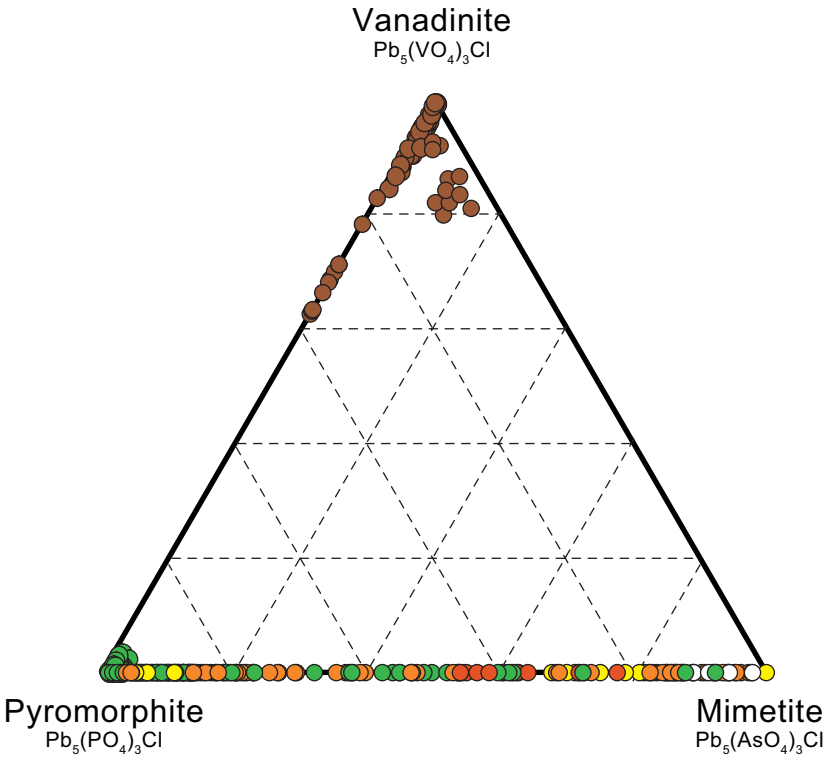
Vanadinite
$Pb_5(VO_4)_3Cl$
Pyromorphite
$Pb_5(PO_4)_3Cl$
Mimetite
$Pb_5(AsO_4)_3Cl$

(B)

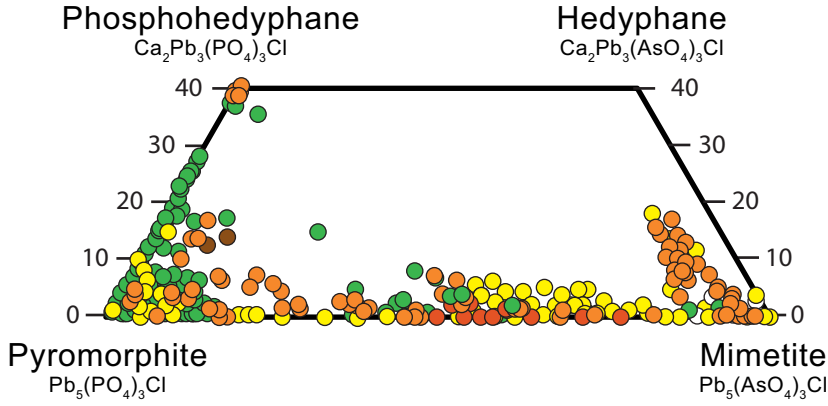
Phosphohedyphane
$Ca_2Pb_3(PO_4)_3Cl$
Hedyphane
$Ca_2Pb_3(AsO_4)_3Cl$
40
30
20
10
0
Pyromorphite
$Pb_5(PO_4)_3Cl$
Mimetite
$Pb_5(AsO_4)_3Cl$

Figure 3 (cont.)

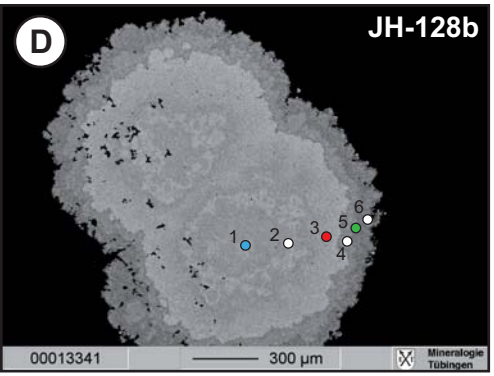

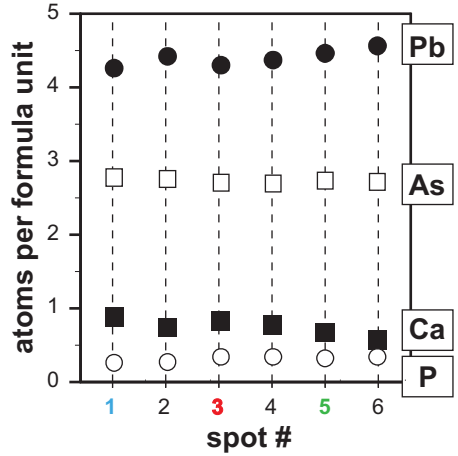

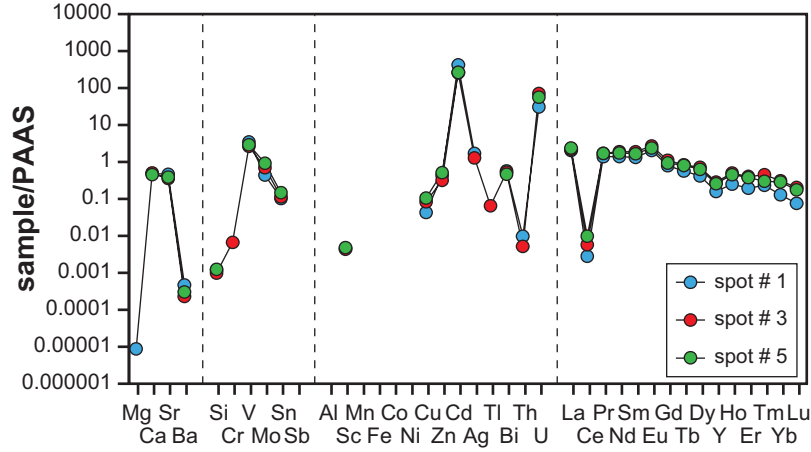

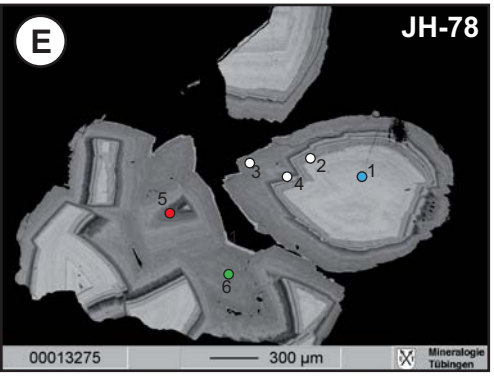

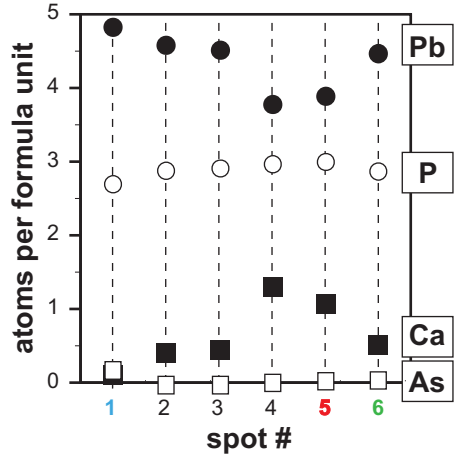

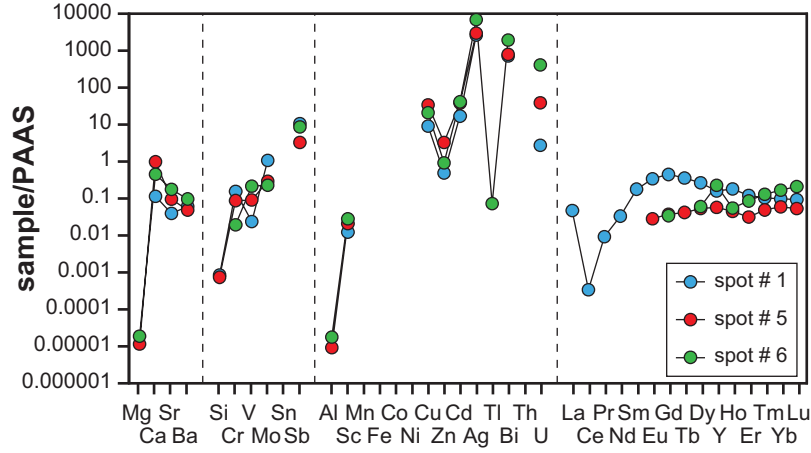

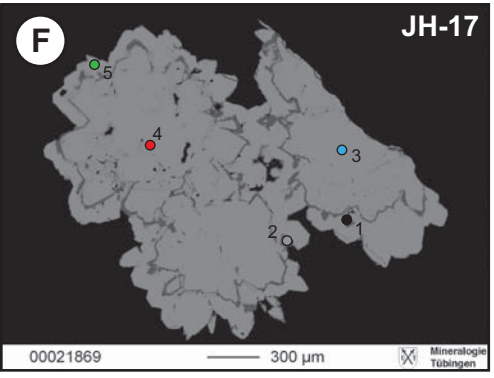

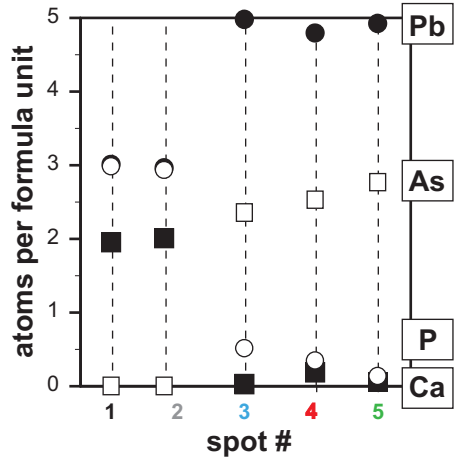

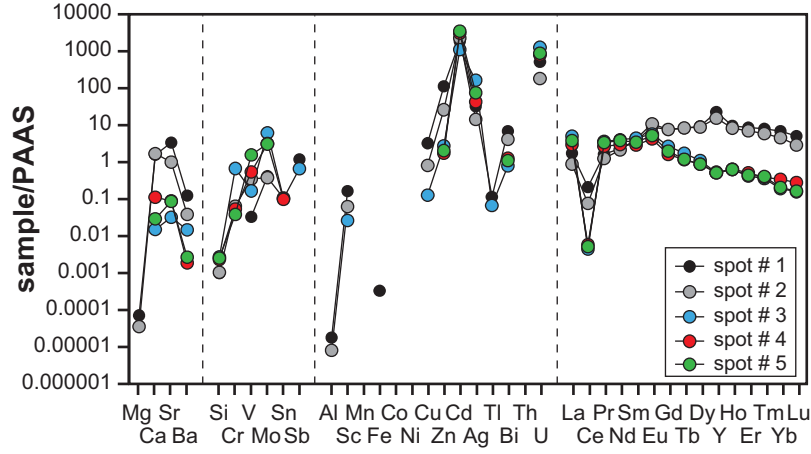

Figure 4

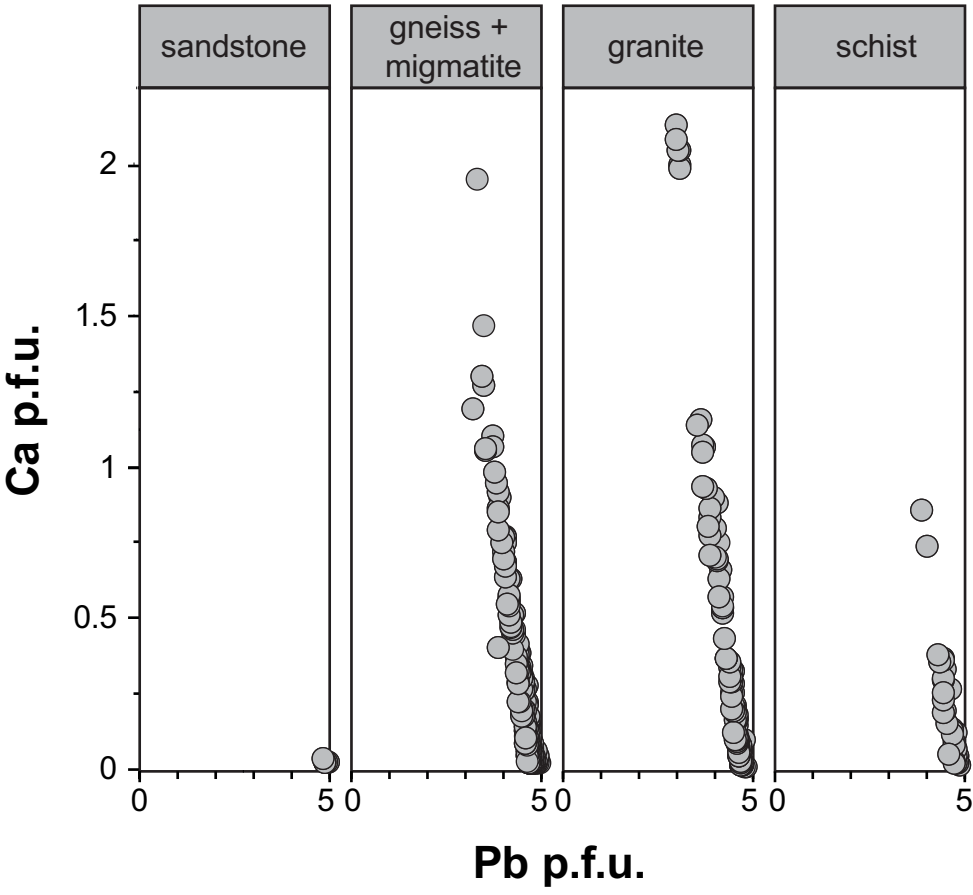
sandstone
gneiss + migmatite
granite
schist
Ca p.f.u.
Pb p.f.u.
0
0.5
1
1.5
2
0
5

Figure 5

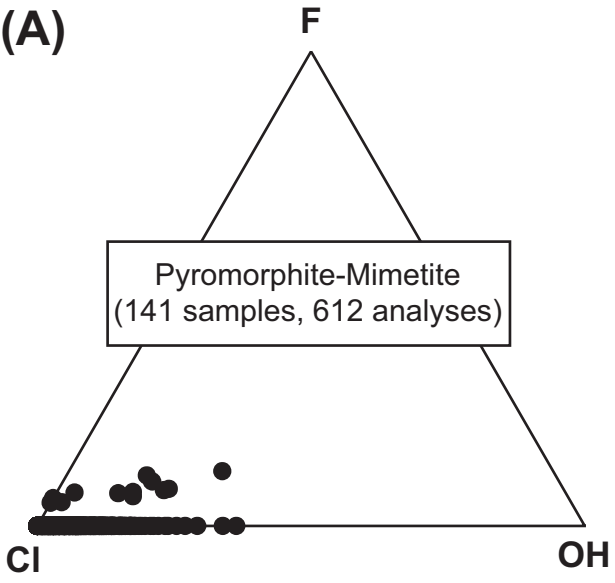
(A)
F
Pyromorphite-Mimetite
(141 samples, 612 analyses)
Cl
OH

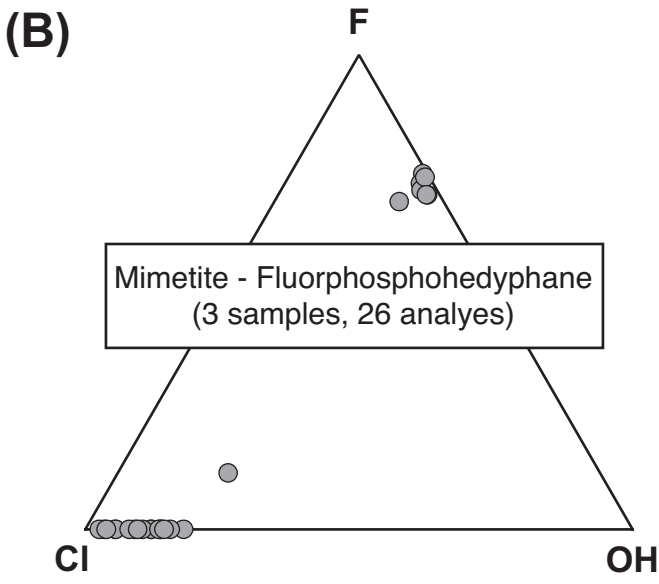
(B)
F
Mimetite - Fluorphosphohedyphane
(3 samples, 26 analyes)
Cl
OH

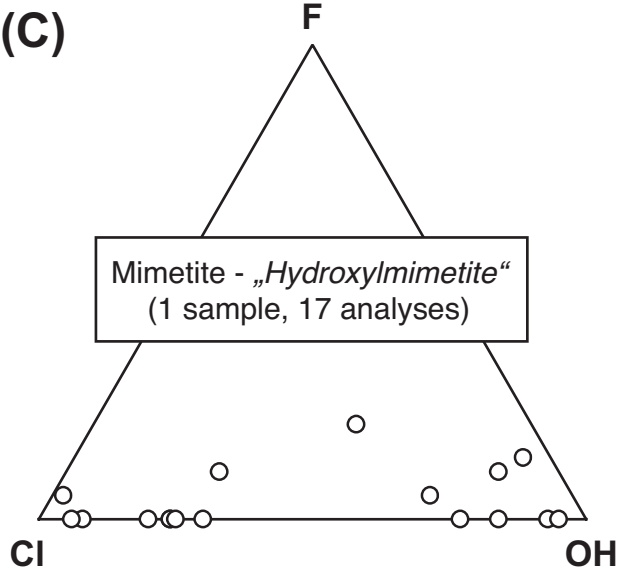
(C)
F
Mimetite - „Hydroxylmimetite“
(1 sample, 17 analyses)
Cl
OH

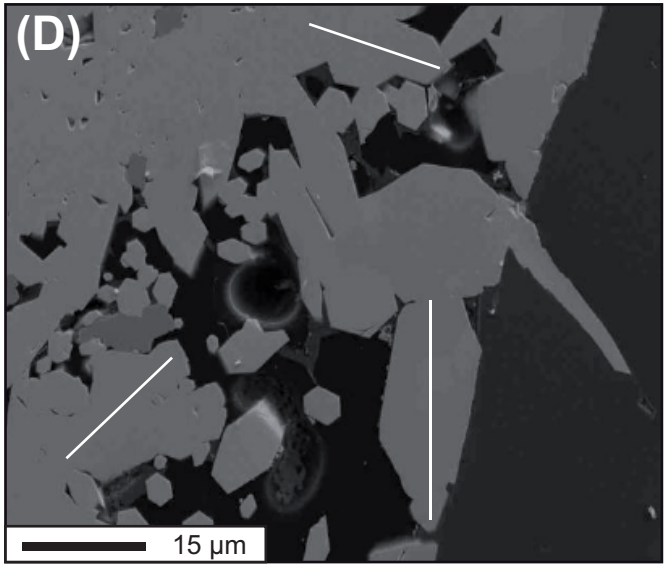
(D)
15 µm

Figure 6

(A)

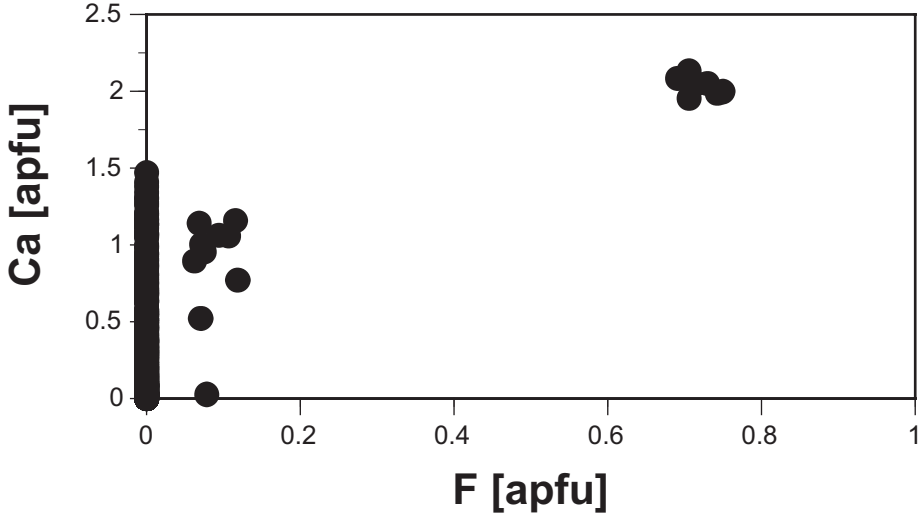
Ca [apfu]
2.5
2
1.5
1
0.5
0
0
0.2
0.4
0.6
0.8
1
F [apfu]

(B)

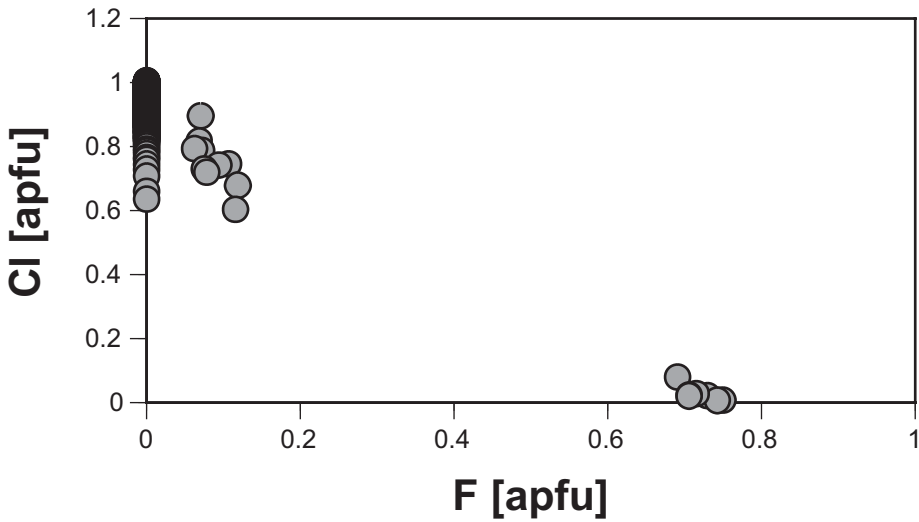
Cl [apfu]
1.2
1
0.8
0.6
0.4
0.2
0
0
0.2
0.4
0.6
0.8
1
F [apfu]

Figure 7

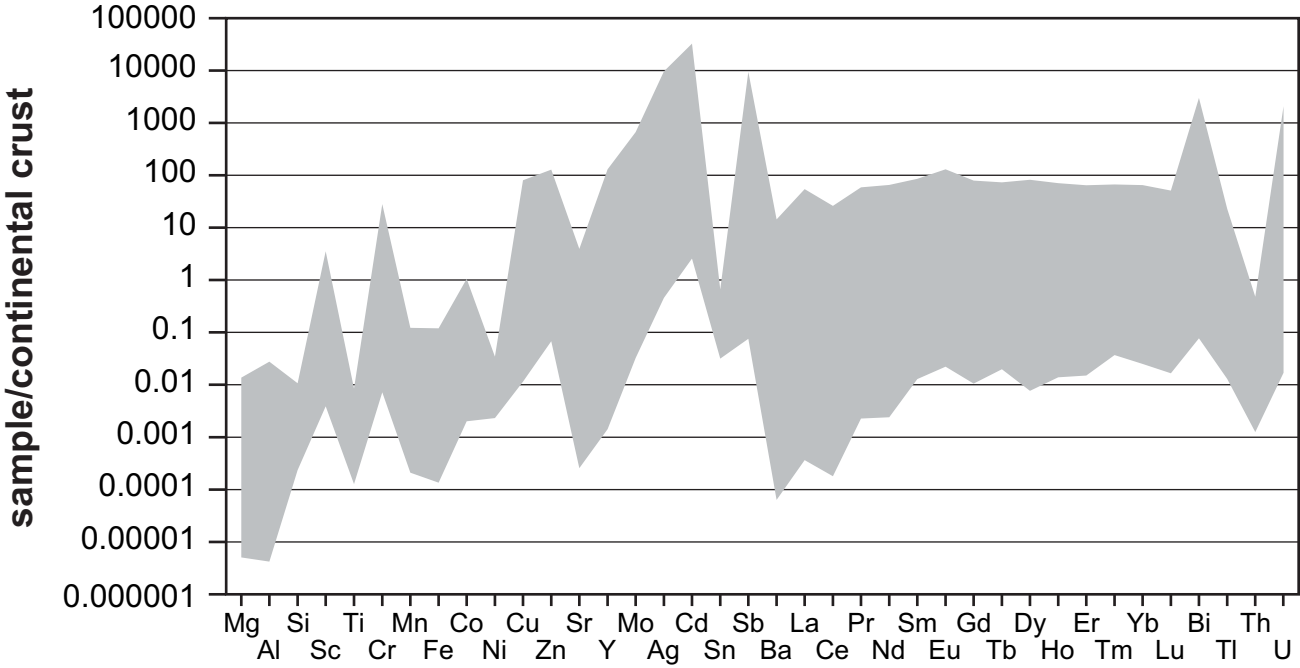
sample/continental crust
100000
10000
1000
100
10
1
0.1
0.01
0.001
0.0001
0.00001
0.000001
Mg Al Si Sc Ti Cr Mn Fe Co Ni Cu Zn Sr Y Mo Ag Cd Sn Sb Ba La Ce Pr Nd Sm Eu Gd Tb Dy Ho Er Tm Yb Lu Bi Tl Th U

Figure 8

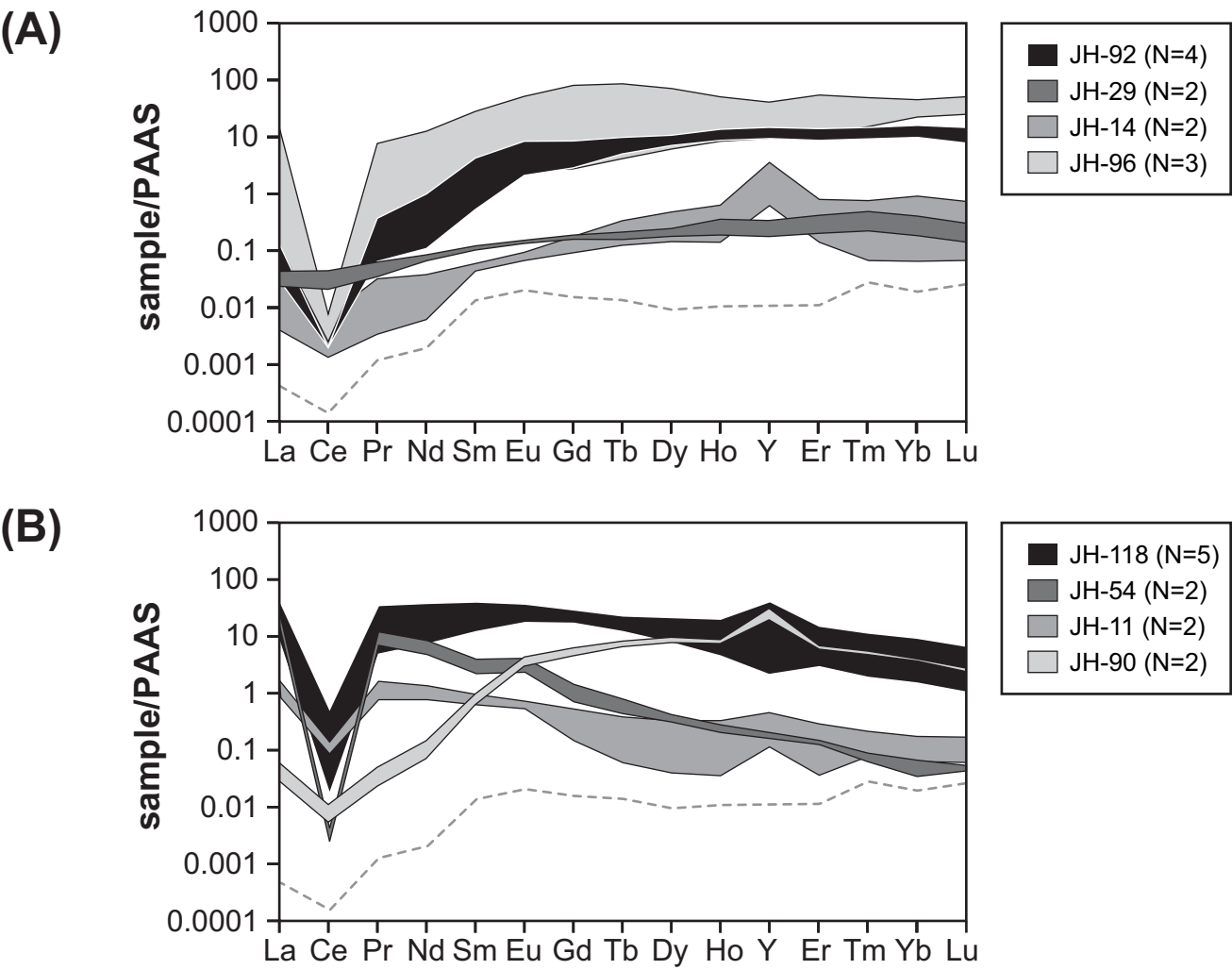
(A)
1000
100
10
1
0.1
0.01
0.001
0.0001
sample/PAAS
La Ce Pr Nd Sm Eu Gd Tb Dy Ho Y Er Tm Yb Lu
JH-92 (N=4)
JH-29 (N=2)
JH-14 (N=2)
JH-96 (N=3)
(B)
1000
100
10
1
0.1
0.01
0.001
0.0001
sample/PAAS
La Ce Pr Nd Sm Eu Gd Tb Dy Ho Y Er Tm Yb Lu
JH-118 (N=5)
JH-54 (N=2)
JH-11 (N=2)
JH-90 (N=2)

Figure 9

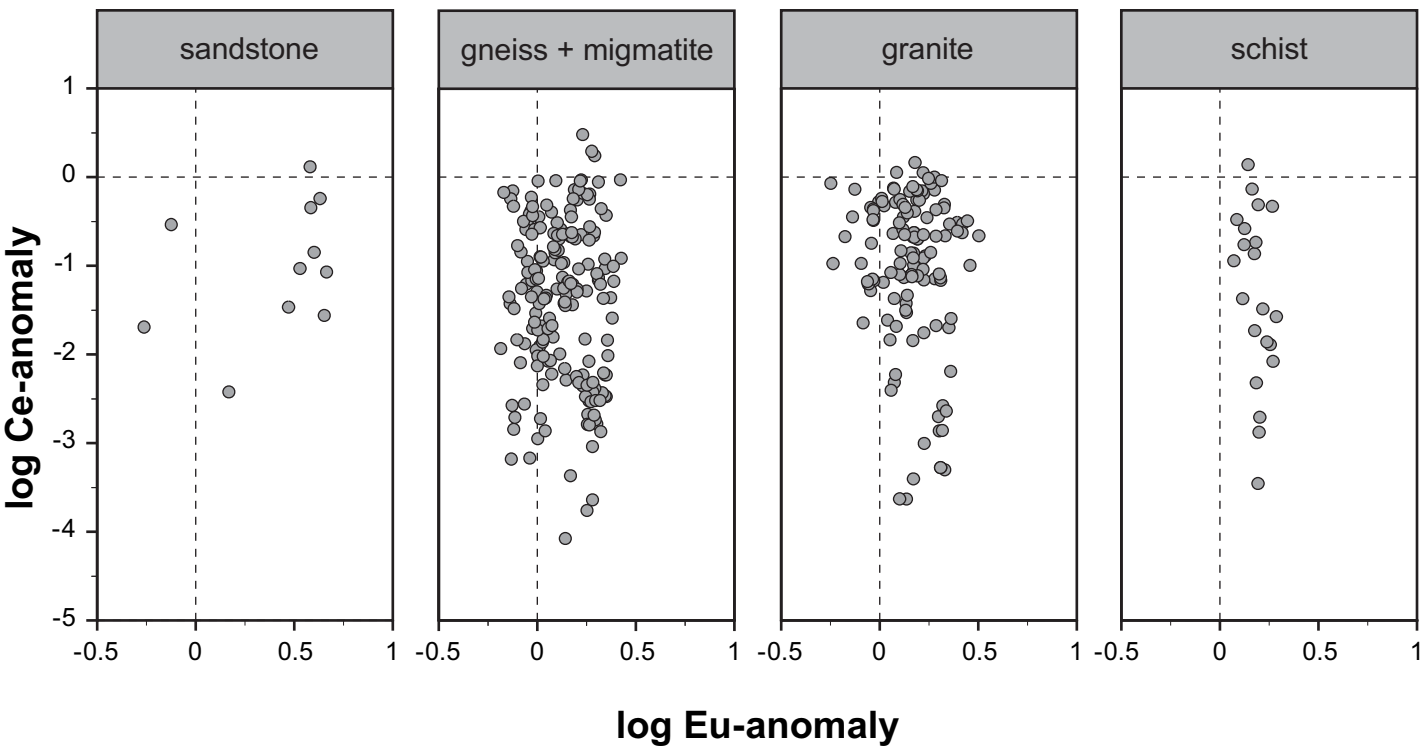
sandstone
gneiss + migmatite
granite
schist
log Ce-anomaly
log Eu-anomaly
1
0
-1
-2
-3
-4
-5
-0.5
0
0.5
1

Figure 10

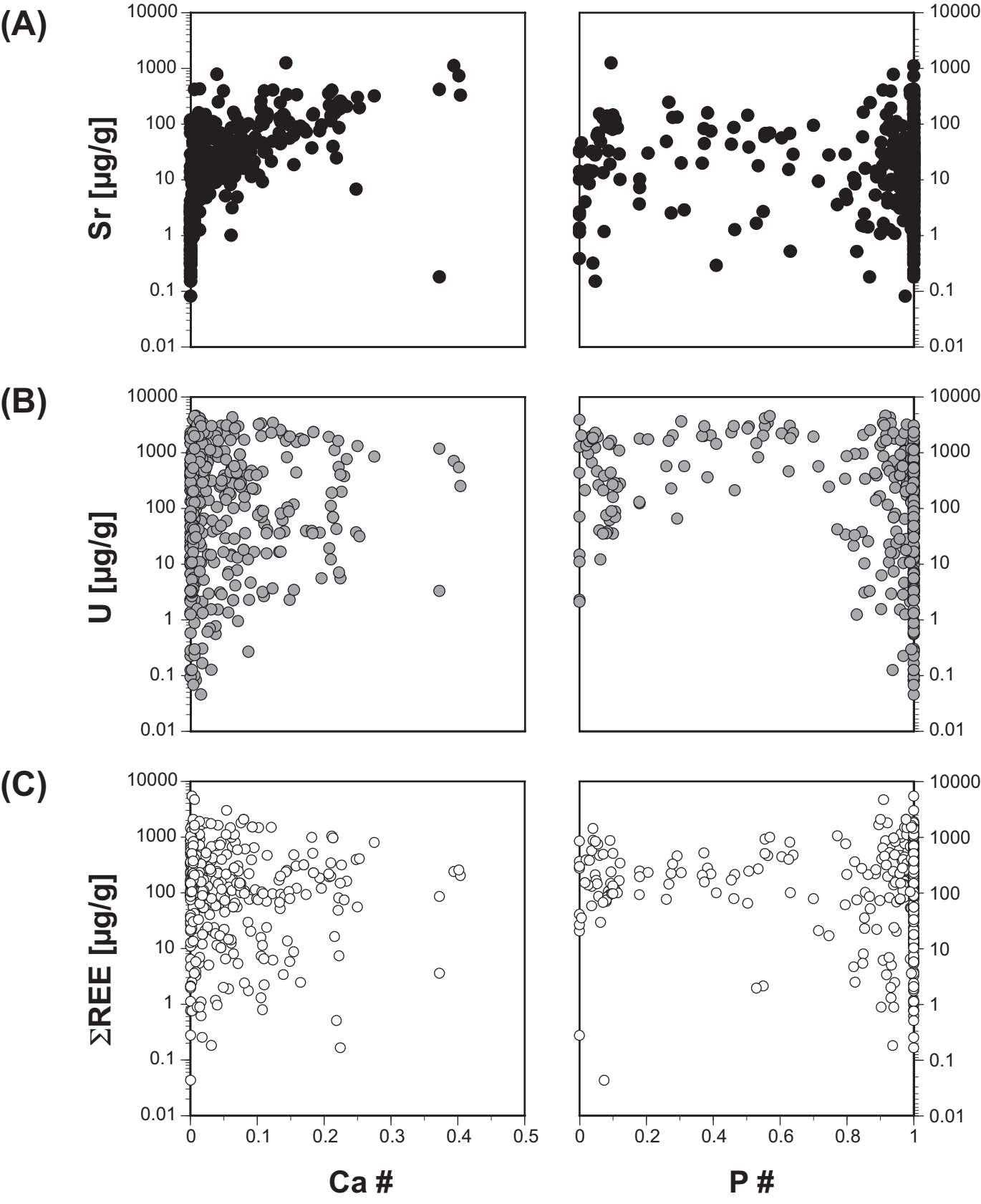
(A)
(B)
(C)
Sr [µg/g]
U [µg/g]
ΣREE [µg/g]
10000
1000
100
10
1
0.1
0.01
0
0.1
0.2
0.3
0.4
0.5
0.6
0.8
1
Ca #
P #

Figure 11

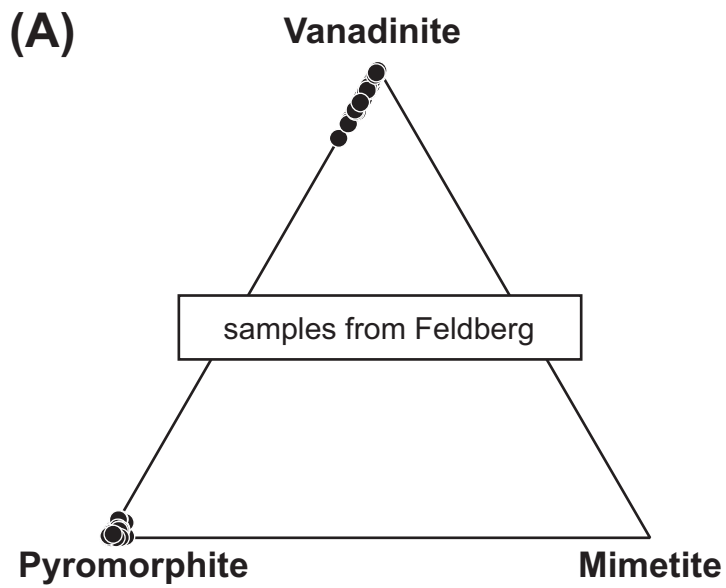
(A)
Vanadinite
samples from Feldberg
Pyromorphite
Mimetite

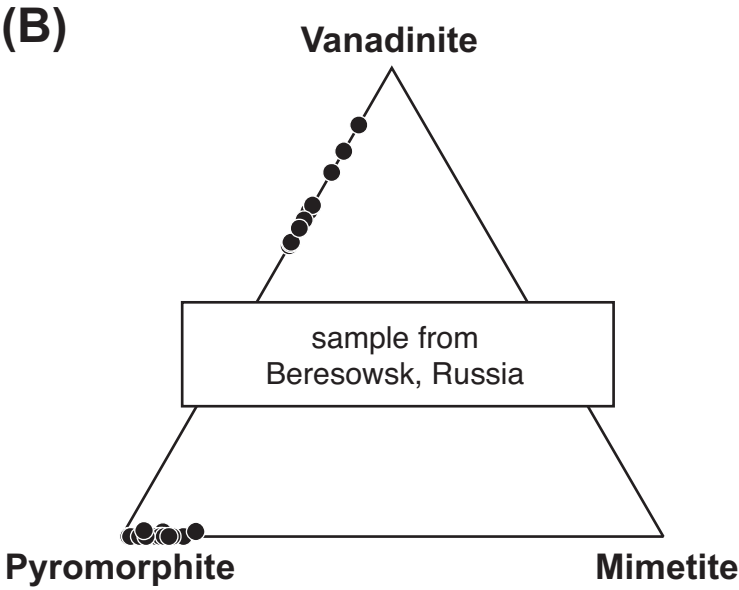
(B)
Vanadinite
sample from
Beresowsk, Russia
Pyromorphite
Mimetite

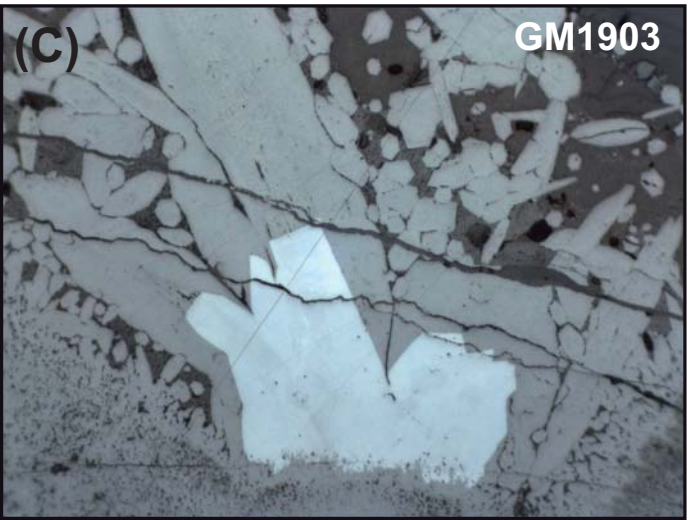
(C)
GM1903


(D)
GM1906

Figure 12

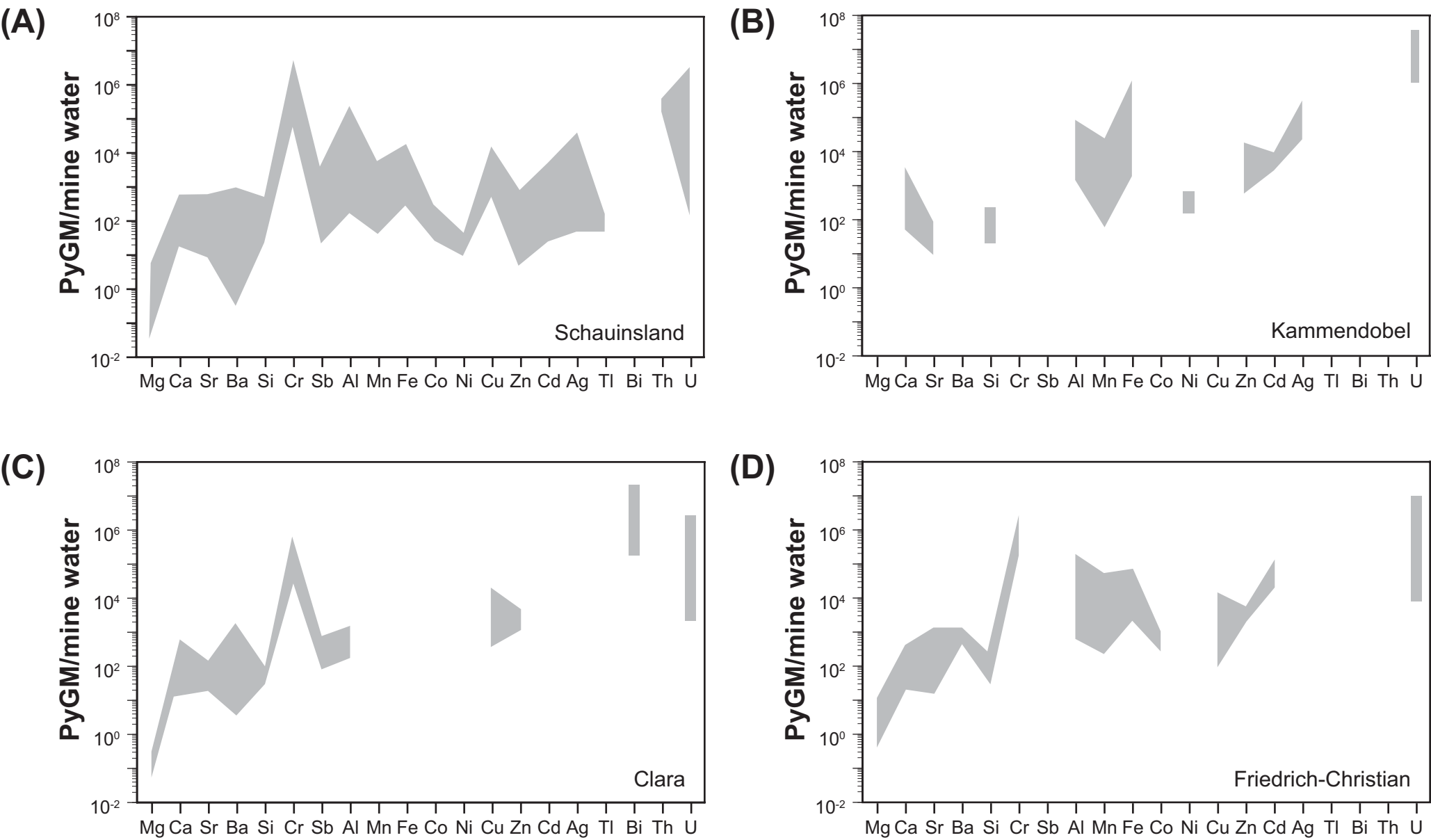
(A)
PyGM/mine water
10^8
10^6
10^4
10^2
10^0
10^{-2}
Mg Ca Sr Ba Si Cr Sb Al Mn Fe Co Ni Cu Zn Cd Ag Tl Bi Th U
Schauinsland
(B)
PyGM/mine water
Mg Ca Sr Ba Si Cr Sb Al Mn Fe Co Ni Cu Zn Cd Ag Tl Bi Th U
Kammendobel
(C)
PyGM/mine water
Mg Ca Sr Ba Si Cr Sb Al Mn Fe Co Ni Cu Zn Cd Ag Tl Bi Th U
Clara
(D)
PyGM/mine water
Mg Ca Sr Ba Si Cr Sb Al Mn Fe Co Ni Cu Zn Cd Ag Tl Bi Th U
Friedrich-Christian

Figure 13

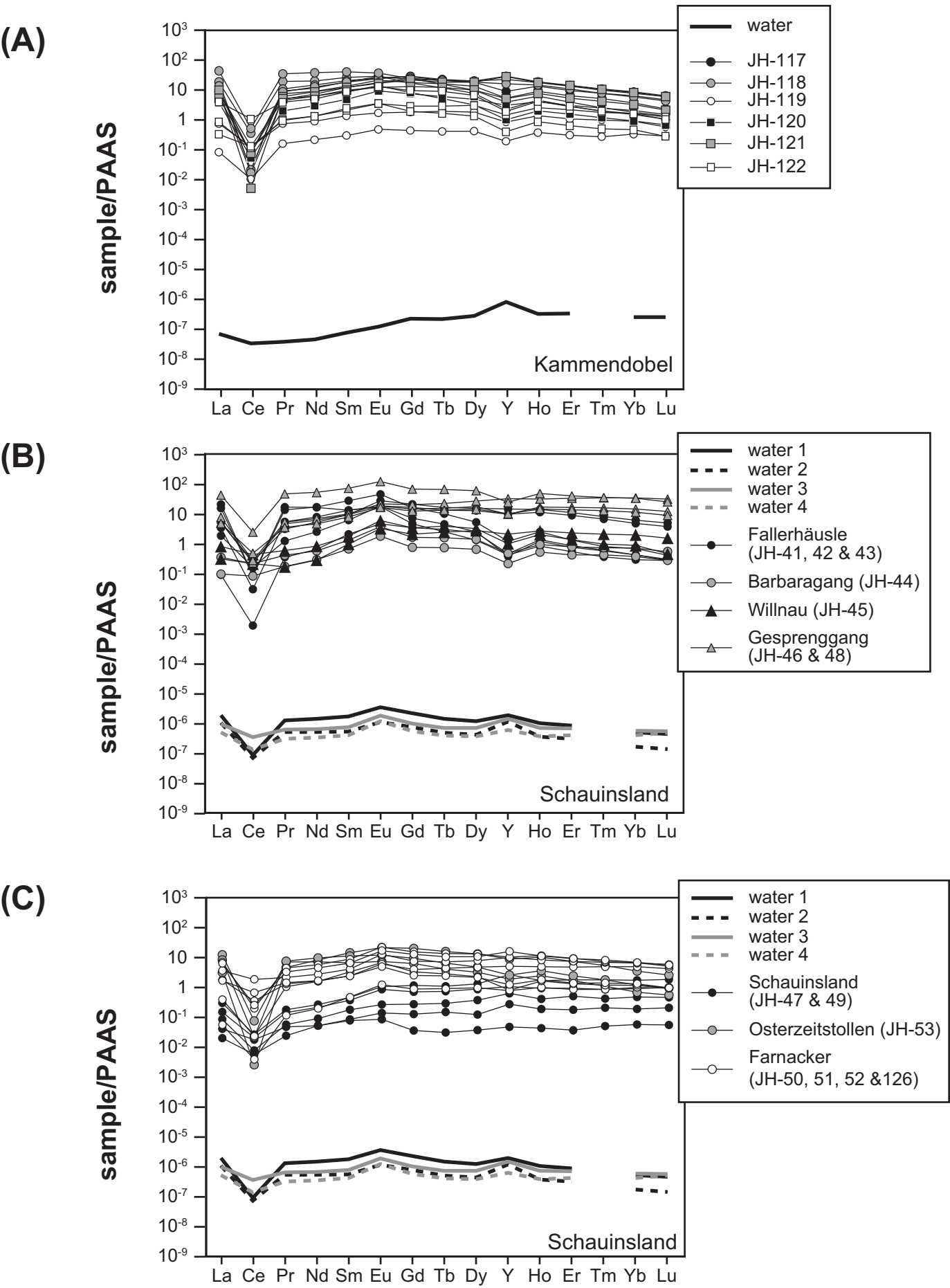
(A)
sample/PAAS
water
JH-117
JH-118
JH-119
JH-120
JH-121
JH-122
Kammendobel
La Ce Pr Nd Sm Eu Gd Tb Dy Y Ho Er Tm Yb Lu
(B)
sample/PAAS
water 1
water 2
water 3
water 4
Fallerhäusle (JH-41, 42 & 43)
Barbaragang (JH-44)
Willnau (JH-45)
Gesprenggang (JH-46 & 48)
Schauinsland
La Ce Pr Nd Sm Eu Gd Tb Dy Y Ho Er Tm Yb Lu
(C)
sample/PAAS
water 1
water 2
water 3
water 4
Schauinsland (JH-47 & 49)
Osterzeitstollen (JH-53)
Farnacker (JH-50, 51, 52 &126)
Schauinsland
La Ce Pr Nd Sm Eu Gd Tb Dy Y Ho Er Tm Yb Lu

Figure 13 (cont.)

(D)

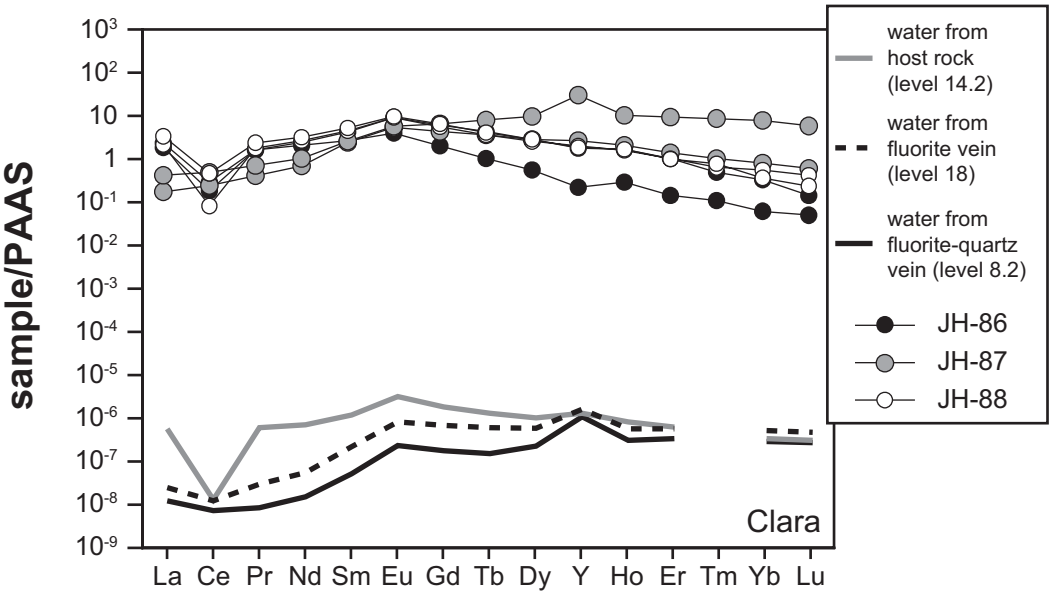

(E)

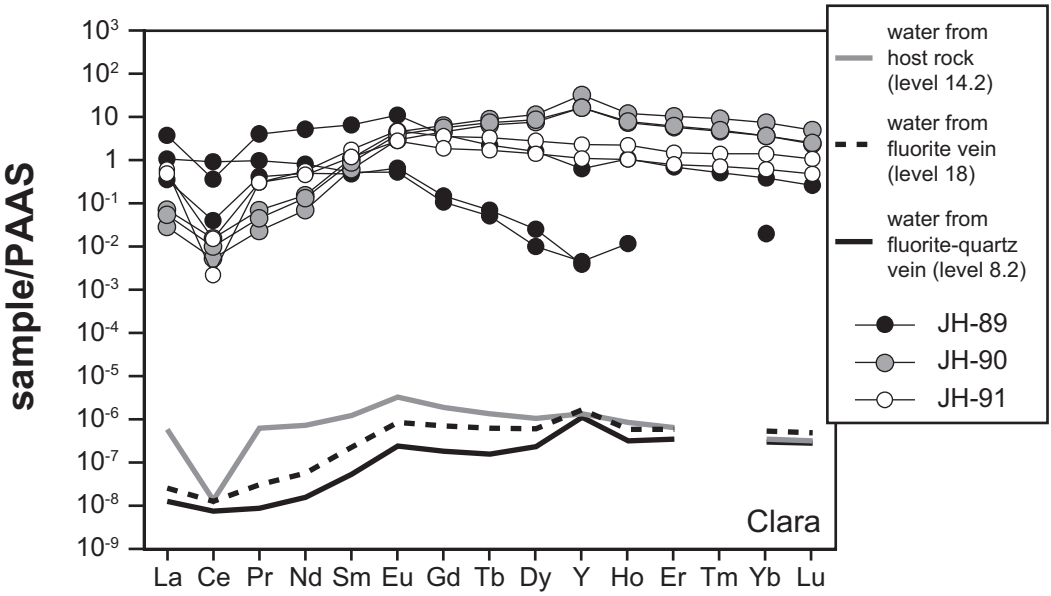

(F)

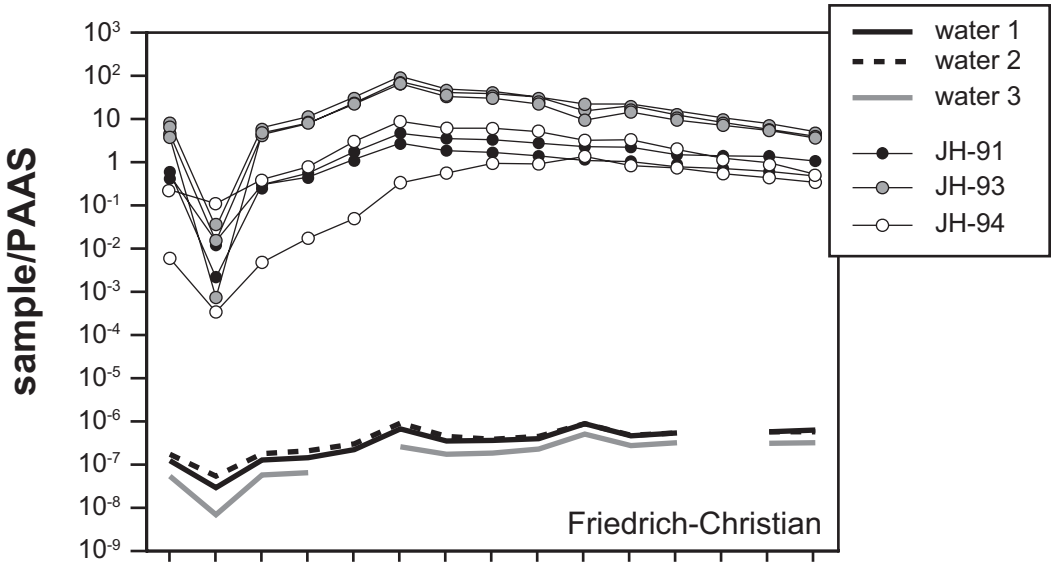

Table 1: Studied pyromorphite-group mineral samples along with localitites (see Fig. **1**), mineralization type (reported in order of decreasing abundance) and host rocks of the respective hydrothermal veins. Bar-barite, Fl-fluorite, Sid-siderite, Goe-goethite, Qtz-quartz, Cal-calcite, Dol-dolomite, Gal-galena, Ccp-chalcopyrite, Fahl-fahlore (tennantite-tetrahedrite solid solution), Sph-sphalerite.

	Locality		Sample numbers	Mineralization type	Host rock
1	Silberbrünnle	Gengenbach, Kinzigtal	JH-78	Qtz-Ccp-Gal-Fahl	Gneiss
2	Clara	Wolfach	JH-86 - 90	Bar-Fl-Qtz-Gal-Fahl-Ccp	Gneiss
3	Friedrich-Christian	Schapbach	JH-91, 93 & 94	Fl-Qtz-Gal-Ccp	Gneiss
4	Herrensegen	Schapbach	JH-92, 95 - 98	Fl-Qtz-Gal-Ccp	Gneiss
5	Erzengel Gabriel	Hausach, Kinzigtal	JH-79 & 80	Fl-Bar-Qtz-Gal	Gneiss
6	Giesenbächle	Lahr	JH-81 - 85	Sid/Goe-Qtz-Bar-Gal	Sandstone
7	Michael	Lahr	JH-74 – 77, LK5-9, GM1928-1939	Bar-Qtz-Gal-Sph-native arsenic	Gneiss & granite
8	Eichhalde	Biberach	JH-101	Qtz-Sid-Fahl-Gal-Ccp	Gneiss & granite
9	Prinzbach	Biberach	JH-99 & 100	Qtz-Sid-Fahl-Gal-Ccp	Gneiss & granite
10	Sankt Josefi	Schuttertal	JH-102	Bar-Qtz-Gal-Sph	Gneiss
11	Silberloch	Freiamt	JH-110 - 113	Bar-Qtz-Gal-(Fahl)	Sandstone
12	Gesprengang	Schauinsland	JH-46 & 48	Qtz-Gal-Sph	Migmatite & gneiss
13	Farnacker	Schauinsland	JH-50 - 52, 126	Qtz-Gal	Migmatite
14	Klöpfe	Riggenbach, Münstertal	JH-72, 73, 125 & 127	Qtz-Bar-Gal	Migmatite
15	Osterzeitstollen	Schauinsland	JH-53	Qtz-Gal-Sph	Migmatite
16	Fallerhäusle	Schauinsland	JH-41 - 43	Qtz-Gal	Migmatite
17	Barbaragang	Schauinsland	JH-44	Qtz-Gal-Sph	Migmatite
18	no exact location	Schauinsland	JH-47 & 49	Qtz-Gal±Sph	Migmatite
19	Willnau	Schauinsland	JH-45	Qtz-Bar-Gal	Migmatite
20	Katzensteig	St. Wilhelm	JH-103 - 106	Qtz-Gal-(Fahl)	Gneiss
21	Kammendobel	Feldberg	JH-117 - 122	Sid/Goe-Gal	Migmatite
22	Todtnauer Hütte	Feldberg	JH-131, GM1901, 1902, 1905, 1906 & 1912	Sid/Goe-Gal	Gneiss
23	Herrenwald	Münstertal	JH-71	Fl-Bar-Qtz-Gal	Gneiss
24	Knappengrund	Münstertal	JH-130	Fl-Bar-Qtz-Gal-Ccp	Gneiss
25	Anton	Wieden	JH-55 - 59	Fl-Bar-Qtz-Gal-Sph-(Ccp)	Gneiss & granite
26	Gauch Süd	Todtnauberg	JH-63	Cal-Qtz-Bar-Fl-Gal	Gneiss
27	Lisbühl Ost	Todtnau	JH-61	Fl-Bar-Qtz-Gal-Ccp	Gneiss

28	Lisbühl West	Todtnau	JH-62	Fl-Bar-Qtz-Gal-Ccp	Gneiss
29	Maus	Todtnau	JH-64	Fl-Bar-Qtz-Gal-Sph	Gneiss
30	Finstergrund	Wieden	JH-60	Fl-Bar-Qtz-Gal	Gneiss
31	Aitern Süd	Schönau	JH-70	Fl-Bar-Qtz-Gal-Sph-Ccp	Schist
32	Pfingstsegen	Schönau	JH-65 - 69	Fl-Bar-Qtz-Gal	Schist
33	Spitzkopf	Neuenweg	JH-115 & 116	Bar-Fl-Gal	Granite
34	Sehringen	Badenweiler	JH-29	Bar-Qtz-Gal	Granite
35	Karlstollen	Badenweiler	JH-36 - 38	Qtz-Bar-Gal	Rhyolite & Schist
36	Altemannfels	Badenweiler	JH-30 – 32, 39, 40 &128	Qtz-Bar-Gal	Gneiss & sandstone
37	Haus Baden	Badenweiler	JH-17 – 22	Qtz-Bar-Fl-Gal-(Sph)-(Ccp)	Granite
38	Wilhelminenstollen	Badenweiler	JH-23 - 28	Qtz-Bar-Gal	Granite
39	Fürstenfreude	Badenweiler	JH-33 - 35	Bar-Qtz-Gal	Gneiss
40	Hermann	Görwihl, Hotzenwald	JH-107 & 108	Fl-Qtz-Bar-Gal	Granite
41	Ruprechtgang	Urberg, St. Blasien	JH-1 – 16, 54 & 129	Fl-Bar-Qtz-Dol-Gal-Sph-Ccp	Gneiss & granite
42	Segalen	Hotzenwald	JH-114	Fl-Bar-Qtz-Gal	Rhyolite
43	Brenden-Mettma	Hotzenwald	JH-124	Fl-Bar-Qtz-Gal	Granite
44	Igelschlatt	Hotzenwald	JH-123	Fl-Bar-Qtz-Gal-Sph-Ccp	Granite

Table 2: Composition of the two calibration materials PYR-1 (pyromorphite) and MIM-1 (mimetite) as determined by AAS and IC, compared to the respective theoretical end member compositions.

	Theoretical pyromorphite end member	PYR-1	Deviation [%]		Theoretical mimetite end member	MIM-1	Deviation [%]
[wt%]							
PbO	82.28	83.16	~1		74.99	73.57	~2
CaO		b.d.l.				0.35	
ZnO		0.06				b.d.l.	
P_2O_5	15.70	15.24	~3			b.d.l.	
As_2O_5		b.d.l.			23.17	23.32	~1
Cl	2.62	2.54	~5		2.38	2.25	~6
O=Cl	-0.59	-0.57			-0.54	-0.51	
Total	100.00	100.43			100.00	98.98	
Formulae based on 8 cations							
Pb	5.00	5.07			5.00	4.90	
Ca						0.09	
Zn		0.01					
Total	**5.00**	**5.08**	~2		**5.00**	**4.99**	<1
P	3.00	2.92					
As					3.00	3.01	
Total	**3.00**	**2.92**	~3		**3.00**	**3.01**	<1
Cl	1.00	0.97	~3		1.00	0.94	~6

Table 3: WDS analysis configuration used in this study for EPMA.

Element	Crystal	Fluorescence line analyzed	Standard	Counting time (peak/background) [s]	Detection limit [ppm]
Pb	PETJ	Mβ	Pyromorphite	30/15	1900
Ca	PETJ	Kα	Apatite	30/15	200
U	PETJ	Mα	UO_2	30/15	700
Cu	LIFH	Kβ	Cu-metal	30/15	2400
Zn	LIFH	Kα	Zn-metal	30/15	400
Fe	LIFH	Kα	Hematite	30/15	270
Ba	PETJ	Lα	Baryte	30/15	570
P	PETJ	Kα	Pyromorphite	30/15	650
As	TAP	Lα	Mimetite	30/15	1200
V	LIFH	Kα	V-metal	30/16	270
Si	TAP	Kα	Diopside	30/15	470
S	PETJ	Kα	Baryte	30/15	650
Cl	PETJ	Kα	Pyromorphite	30/15	210
F	LDE1	Kα	Apatite	60/30	900

Table 4: Results for our analyses of NIST SRM6102 glass, compared to the literature values (Pearce et al., 1997; GEOREM database).

	Literature value	Own analyses (N=24)		
		Mean value	1σ	Deviation [%]
Mg	68	63	4	-7
Al	10750	10480	670	-3
Si	337000	346350	22200	+3
P	46.6	45	5	-6
Sc	39.9	39	2	-3
Ti	48.1	44	1	-9
V	38.8	38	2	-3
Cr	36.4	38	2	+4
Mn	38.7	37	2	-4
Fe	51	50	5	-2
Co	35.5	35	2	±0
Ni	38.8	39	1	±0
Cu	37.8	39	2	+4
Zn	39.1	41	4	+5
As	35.7	37	3	+4
Sr	78.4	76	2	-4
Y	38.3	37	1	-5
Mo	37.4	35	1	-7
Ag	22	23	1	+5
Cd	28.1	29	1	+2
Sn	38.6	37	2	-4
Sb	34.7	32	2	-8
Ba	39.3	38	3	-4
La	36	37	1	+3
Ce	38.4	39	2	+2
Pr	37.9	37	1	-3
Nd	35.5	36	2	+1
Sm	37.7	37	1	+2
Eu	35.6	37	2	+4
Gd	37.3	35	1	-5
Tb	37.6	37	1	±0
Dy	35.5	34	1	-4
Ho	38.3	36	1	-7
Er	38	37	1	-3
Tm	36.8	35	1	-5
Yb	39.2	38	1	-3
Lu	37	35	1	-6
Tl	14.9	20	1	+34
Bi	30.2	32	1	+6
Th	37.8	37	1	-2
U	37.4	38	1	+2

Table 5: Representative analyses of pyromorphite-group minerals from the Schwarzwald, Southwestern Germany. Major and minor elements were determinded by EPMA, trace elements by LA-ICP-MS.

	JH-96-1	JH-96-6	JH-114-1	JH-114-2	JH-114-4	JH-114-6	JH-128-4	JH-129-1	JH-129-5	JH-129-6
wt %										
SiO_2	b.d.l.	b.d.l	b.d.l	b.d.l	0.08	b.d.l	b.d.l	b.d.l	0.53	0.10
PbO	81.44	73.95	70.48	70.62	77.34	78.36	71.09	64.21	76.49	75.38
CaO	0.62	4.92	3.96	2.95	0.34	0.30	3.09	10.44	0.61	3.30
FeO	b.d.l	b.d.l	b.d.l	b.d.l	b.d.l	b.d.l	b.d.l	b.d.l	b.d.l	b.d.l
ZnO	b.d.l	b.d.l	b.d.l	b.d.l	b.d.l	0.12	b.d.l	b.d.l	b.d.l	b.d.l
CuO	b.d.l	0.20	b.d.l	b.d.l	b.d.l	b.d.l	b.d.l	0.31	b.d.l	b.d.l
UO_2	b.d.l	b.d.l	b.d.l	0.15	0.09	0.20	b.d.l	0.16	0.30	0.16
BaO	b.d.l	0.11	b.d.l	b.d.l	b.d.l	b.d.l	b.d.l	b.d.l	b.d.l	b.d.l
P_2O_5	14.41	16.22	1.56	1.49	1.26	4.03	1.64	17.04	6.84	11.10
As_2O_5	1.63	1.09	23.43	23.44	21.78	16.96	22.49	5.58	11.92	7.53
V_2O_5	b.d.l	b.d.l	0.09	b.d.l	b.d.l	b.d.l	b.d.l	b.d.l	b.d.l	0.16
SO_3	b.d.l	b.d.l	b.d.l	b.d.l	b.d.l	b.d.l	b.d.l	b.d.l	b.d.l	b.d.l
Cl	2.28	2.68	2.48	2.37	2.28	2.36	2.34	0.08	2.10	1.84
F	b.d.l	b.d.l	b.d.l	b.d.l	b.d.l	b.d.l	b.d.l	1.19	b.d.l	0.17
Total	100.39	98.97	101.91	101.32	102.99	102.09	100.66	99.28	98.48	99.73
Normalized to (Pb + Ca + U + Zn + Cu + Fe + Ba + P + As + V + S + Si) = 8 apfu										
Pb	4.92	4.01	4.12	4.26	4.94	4.99	4.30	3.00	4.87	4.34
Ca	0.15	1.06	0.92	0.71	0.09	0.08	0.74	1.94	0.15	0.76
Fe										
U				0.01	0.00	0.01		0.01	0.02	0.01
Zn						0.02				
Cu		0.03						0.04		
Ba		0.01								
Sum	5.07	5.11	5.04	4.97	5.03	5.10	5.04	4.99	5.03	5.10
P	2.74	2.77	0.29	0.28	0.25	0.81	0.31	2.50	1.37	2.01
As	0.19	0.11	2.66	2.74	2.70	2.10	2.64	0.51	1.47	0.84
V			0.01							0.02
Si					0.02				0.12	0.02
S										
Sum	2.93	2.88	2.96	3.03	2.97	2.90	2.96	3.01	2.97	2.90
Cl	0.87	0.91	0.91	0.90	0.91	0.95	0.89	0.02	0.84	0.67
F								0.65		0.11
OH	0.13	0.09	0.09	0.10	0.09	0.05	0.11	0.32	0.16	0.22
wt.% H_2O	0.09	0.06	0.06	0.07	0.05	0.03	0.07	0.28	0.10	0.15
O=F,Cl	0.52	0.60	0.56	0.54	0.51	0.53	0.53	0.52	0.47	0.49
Total corrected	99.96	98.43	101.42	100.85	102.53	101.59	100.20	99.04	98.11	99.40
µg/g										
Mg		1.2	0.9	3.3				12.9	0.6	0.7
Sr	14	220	146	1254	33	132	108	418	87	95
Ba	224	441	0.5	60.2	0.8	24	0.1	339	126	185
Cr	50	3.8		2.9	10.2	26.6	0.8	14.9	258	233
Mo			0.3	0.5	2.6	2.1	0.5	1.2	10.0	3.2
Sb	1.6	0.7		0.5		0.5		9.9	2.4	2.9
Si	382	160	209	200	734	392	262	390	2600	511
V	2.2	3.0	511	12.4	32	245	351	63	9.2	820
Al	3.7	1.4		5.4		0.7		2.4	2.0	1.3
Sc	28	33	0.1	7.9	0.1	4.6	0.1	0.2		0.2
Mn			0.4	18.2						
Fe				9.1				31		10.4
Co				2.5						
Ni				0.3						
Cu	330	1457	2.0	129	2.5	18.4	2.1	2242	100	184
Zn	10.3	20.6	46	195	134	734	21.9	311	39	67

Cd		0.7	46	220	171	123	20	20	10.8	6.9
Ag	67	29	0.1	5.9	2.7	8.1	0.1	15.9	17.0	20
Sn	0.2	0.2	0.2				0.2	0.3		0.1
Tl				0.3	0.1	0.1	0.0			
Bi	40.5	76	0.1	2.2	0.2	0.3	0.1	4.0	1.1	1.0
Th			0.0				0.0		0.0	
U	14.7	19.2	36	1640	1457	2065	88	1179	3022	1948
La	194	4.7	233	35	34	124	42	0.3	41	13.7
Ce	3.5	0.2	0.2	1.1		0.1	0.2	0.1	8.1	2.0
Pr	48	2.0	44	7.9	8.0	21.1	8.0	0.0	5.6	2.8
Nd	306	12.8	174	45	40	98	36	0.2	18.8	16.2
Sm	140	6.3	30	15.9	8.6	19.7	7.0	0.1	2.3	5.3
Eu	61	2.8	11.0	8.6	3.9	8.8	2.8	0.1	0.6	3.0
Gd	245	12.8	11.8	26	5.3	21.5	3.9	0.3	0.8	9.4
Tb	49	3.2	1.2	4.3	0.6	3.3	0.5	0.1	0.1	1.9
Dy	321	28	4.3	30	3.5	18.5	2.5	0.7	0.6	12.1
Y	851	251	8.5	757	11.7	119	5.1	34	9.8	118
Ho	59	8.3	0.5	7.4	0.6	3.3	0.4	0.2	0.1	2.4
Er	145	31	0.8	23	1.2	6.6	0.8	0.6	0.3	5.6
Tm	20	6.1	0.1	3.4	0.2	0.6	0.1	0.1	0.0	0.6
Yb	129	63	0.3	26	0.9	3.3	0.6	0.8	0.2	3.4
Lu	15.8	10.8	0.0	3.7	0.1	0.4	0.1	0.1	0.0	0.4

Table 6: Electron microprobe analyses of vanadinites and of mimetite-"*hydroxylmimetite*" solid solutions from the Schwarzwald.

	GM1906_2	GM1912_14	GM1905_11	JH-53-2	JH-54-3	LK9_29	LK9_8	LK9_10	LK9_16	LK9_22
wt %										
SiO_2	b.d.l.	b.d.l.	b.d.l.	b.d.l.	b.d.l.	b.d.l.	b.d.l.	b.d.l.	b.d.l.	b.d.l.
PbO	79.56	80.29	78.75	78.87	79.44	73.83	74.35	75.26	76.71	76.04
CaO	0.02	b.d.l.	0.32	b.d.l.	b.d.l.	0.01	0.04	b.d.l.	b.d.l.	b.d.l.
FeO	0.04	b.d.l.	b.d.l.	b.d.l.	b.d.l.	b.d.l.	b.d.l.	b.d.l.	b.d.l.	b.d.l.
ZnO	b.d.l.	b.d.l.	b.d.l.	b.d.l.	b.d.l.	0.32	0.11	b.d.l.	b.d.l.	0.05
CuO	0.13	0.19	b.d.l.	b.d.l.	b.d.l.	b.d.l.	b.d.l.	b.d.l.	b.d.l.	b.d.l.
UO_2	b.d.l.	b.d.l.	0.16	0.19	b.d.l.	0.96	0.24	b.d.l.	0.30	0.32
BaO	b.d.l.	b.d.l.	b.d.l.	b.d.l.	b.d.l.	b.d.l.	b.d.l.	b.d.l.	b.d.l.	b.d.l.
P_2O5	0.61	0.11	2.31	0.49	0.54	0.36	0.24	0.14	0.11	b.d.l.
As_2O_5	0.04	b.d.l.	b.d.l.	1.01	0.87	22.96	22.31	23.00	21.64	21.21
V_2O_5	18.14	19.17	17.16	18.00	18.36	b.d.l.	b.d.l.	b.d.l.	b.d.l.	0.03
SO_3	b.d.l.	b.d.l.	b.d.l.	b.d.l.	b.d.l.	b.d.l.	b.d.l.	b.d.l.	0.16	0.53
Cl	2.33	2.31	2.40	2.29	2.37	1.81	2.22	0.16	0.53	0.77
F	b.d.l.	b.d.l.	b.d.l.	b.d.l.	b.d.l.	b.d.l.	b.d.l.	b.d.l.	b.d.l.	0.25
Total	100.88	102.17	101.10	100.85	101.59	100.25	99.50	98.56	99.45	99.21
Normalized to (Pb + Ca + U + Zn + Cu + Fe + Ba + P + As + V + S + Si) = 8 apfu										
Pb	5.02	5.00	4.86	4.98	4.97	4.87	5.00	5.00	5.12	5.10
Ca	0.01		0.08			0.00	0.01			b.d.l.
Fe	0.01									
Zn						0.06	0.02			0.01
Cu	0.02	0.03								
U			0.01	0.01		0.05	0.01		0.02	0.02
Sum	5.06	5.03	4.95	4.99	4.97	4.98	5.04	5.00	5.14	5.13
P	0.12	0.02	0.45	0.10	0.11	0.07	0.05	0.03	0.02	
As	0.01			0.12	0.11	2.94	2.91	2.97	2.81	2.76
V	2.81	2.95	2.60	2.79	2.82					0.01
S									0.03	0.10

Sum	2.94	2.97	3.05	3.01	3.03	3.02	2.96	3.00	2.86	2.87
Cl	0.93	0.91	0.93	0.91	0.93	0.75	0.94	0.07	0.22	0.32
F										0.20
OH	0.07	0.09	0.07	0.09	0.07	0.25	0.06	0.93	0.78	0.48
wt.% H_2O	0.05	0.06	0.04	0.06	0.04	0.15	0.04	0.57	0.47	0.29
O=F,Cl	0.53	0.52	0.54	0.52	0.54	0.41	0.50	0.04	0.12	0.28
Total corrected	100.40	101.71	100.63	100.38	100.09	99.99	99.04	99.09	99.80	99.22

Table 7: Overview on the minor and trace element contents of pyromorphite-group minerals from the Schwarzwald. „% b.d.l. = percentage of analyses below the respective detection limit.

	range	median	% b.d.l.
Mg	0.08 - 205	0.9	49
Al	0.3 - 2240	4.8	25
Si	73 - 3340	250	9
Sc	0.05 - 50	1.1	24
Ti	0.5 – 32	2.7	77
Cr	0.7 - 2600	58	9
Mn	0.2 - 94	1.9	76
Fe	5.3 - 4680	25	64
Co	0.03 – 18.2	0.2	86
Ni	0.1 – 1.6	0.5	93
Cu	0.3 - 2240	15.1	9
Zn	4.5 - 8570	91	12
Sr	0.08 - 1250	18.7	<1
Y	0.03 - 2735	51	<1
Mo	0.04 - 735	1.3	16
Ag	0.02 - 510	18.1	6
Cd	0.2 - 2920	2.9	9
Sn	0.07 – 1.4	0.2	47
Sb	0.03 - 3770	1.4	26
Ba	0.04 - 8970	38	3
La	0.01 - 1680	25	<1
Ce	0.01 - 1640	2.7	<1
Pr	0.02 - 420	7.0	<1
Nd	0.06 - 1770	35	<1
Sm	0.06 - 400	10.3	<1
Eu	0.02 - 130	4.9	<1
Gd	0.04 - 317	15	<1
Tb	0.01 – 51.4	2.6	<1
Dy	0.03 - 321	13	<1
Ho	0.01 – 58.5	2.2	<1
Er	0.03 - 148	4.9	<1
Tm	0.01 – 19.9	0.6	<1
Yb	0.05 - 129	2.8	<1
Lu	0.01 – 15.8	0.3	<1
Tl	0.01 – 20.6	0.1	73
Bi	0.01 - 480	0.2	14
Th	0.01 – 5.1	0.1	77
U	0.05 - 5590	165	2

Table 8: Overview on the minor and trace element contents of pyromorphite-group minerals from the Schwarzwald.

	range	median	% b.d.l.
Mg	0.08 - 205	0.9	49
Al	0.3 - 2240	4.8	25
Si	73 - 3340	250	9
Sc	0.05 - 50	1.1	24
Ti	0.5 – 32	2.7	77
Cr	0.7 - 2600	58	9
Mn	0.2 - 94	1.9	76
Fe	5.3 - 4680	25	64
Co	0.03 – 18.2	0.2	86
Ni	0.1 – 1.6	0.5	93
Cu	0.3 - 2240	15.1	9
Zn	4.5 - 8570	91	12
Sr	0.08 - 1250	18.7	<1
Y	0.03 - 2735	51	<1
Mo	0.04 - 735	1.3	16
Ag	0.02 - 510	18.1	6
Cd	0.2 - 2920	2.9	9
Sn	0.07 – 1.4	0.2	47
Sb	0.03 - 3770	1.4	26
Ba	0.04 - 8970	38	3
La	0.01 - 1680	25	<1
Ce	0.01 - 1640	2.7	<1
Pr	0.02 - 420	7.0	<1
Nd	0.06 - 1770	35	<1
Sm	0.06 - 400	10.3	<1
Eu	0.02 - 130	4.9	<1
Gd	0.04 - 317	15	<1
Tb	0.01 – 51.4	2.6	<1
Dy	0.03 - 321	13	<1
Ho	0.01 – 58.5	2.2	<1
Er	0.03 - 148	4.9	<1
Tm	0.01 – 19.9	0.6	<1
Yb	0.05 - 129	2.8	<1
Lu	0.01 – 15.8	0.3	<1
Tl	0.01 – 20.6	0.1	73
Bi	0.01 - 480	0.2	14
Th	0.01 – 5.1	0.1	77
U	0.05 - 5590	165	2